GASIFICATION TRANSPORT: A MULTIPHASE CFD APPROACH & MEASUREMENTS

ILLINOIS INSTITUTE OF TECHNOLOGY

FINAL TECHNICAL REPORT

FEBRUARY 15, 2006 TO FEBRUARY 14, 2009

DR. DIMITRI GIDASPOW, PRINCIPAL INVESTIGATOR
VEERAYA JIRADILOK, PH.D.
MAYANK KASHYAP, PH.D. CANDIDATE
BENJAPON CHALERMSINSUWAN, PH.D. CANDIDATE

DE-FG26-06NT42736

ILLINOIS INSTITUTE OF TECHNOLOGY
CHEMICAL AND BIOLOGICAL ENGINEERING DEPARTMENT
10 W 33RD ST
CHICAGO, IL 60616

JULY 31, 2009

DISCLAIMER

TABLE OF CONTENT

ABSTRACT

OBJECTIVE

The objective of this project was to develop predictive theories for the dispersion and mass transfer coefficients and to measure them in the turbulent fluidization regime, using existing facilities. A second objective was to use our multiphase CFD tools to suggest optimized gasifier designs consistent with aims of Future Gen.

CONCLUSIONS

We have shown that the kinetic theory based CFD codes correctly compute:

(1) Dispersion coefficients

(2) Mass transfer coefficients

Hence, the kinetic theory based CFD codes can be used for fluidized bed reactor design without any such inputs.

We have also suggested a new energy efficient method of gasifying coal and producing electricity using a molten carbonate fuel cell. The principal product of this new scheme is carbon dioxide which can be converted into useful products such as marble, as is done very slowly in nature. We believe this scheme is a lot better than the cancelled FutureGen, since the carbon dioxide is safely sequestered.

Title: GASIFICATION TRANSPORT: A MULTIPHASE CFD APPROACH & MEASUREMENTS

Author(s): Dimitri Gidaspow, Veeraya Jiradilok and Mayank Kashyap
Ph.D. students: Mayank Kashyap and Benjapon Chalermsinsuwan
Illinois Institute of Technology
Chemical & Biological Engineering Department
10 West 33rd Street
Chicago, IL 60616
Tel 312-567-3045
Fax 312-567-8874
Email : gidaspow@iit.edu
Grant Number: DE-FG26-06NT42736
Performance Period: 2/15/06 – 12/15/08

OBJECTIVE

The objective of this project was to develop predictive theories for the dispersion and mass transfer coefficients and to measure them in the turbulent fluidization regime, using existing facilities. A second objective was to use our multiphase CFD tools to suggest optimized gasifier designs consistent with aims of Future Gen.

SUMMARY OF ACCOMPLISHMENTS

• **Dispersion coefficients**

The dispersion coefficient is a measure of the quality of mixing. We have identified two types of solids dispersion coefficients: those due to random particle oscillations, “laminar” type, and those due to cluster or bubble motion, “turbulent” type. A literature review shows that dispersion coefficients in fluidized beds differ by more than five orders of magnitude. To understand the phenomena, two types of hydrodynamics models that compute turbulent and bubbling behavior were used to estimate radial and axial gas and solids dispersion coefficients. The

autocorrelation technique was used to compute the dispersion coefficients from the respective computed turbulent gas and particle velocities.

The computations show that the gas and the solids dispersion coefficients are close to each other in agreement with measurements. The simulations show that the radial dispersion coefficients in the riser are two to three orders of magnitude lower that the axial dispersion coefficients, but less than an order of magnitude lower for the bubbling bed at atmospheric pressure. The dispersion coefficients for the bubbling bed at 25 atmospheres are much higher than at atmospheric pressure due to the high bed expansion with smaller bubbles. The computed dispersion coefficients are in reasonable agreement with the experimental measurements reported over the last half century and those measured at IIT and in the NETL riser in Morgantown (Jiradilok et al., 2007, 2008).

• **Optimized gasifier designs (Gasifier – fuel cell)**

For carbon capture fossil fuel electric power generation plants will have to be made more efficient. Department of Energy vision 21 concept involves coal gasification with oxygen in an entrained flow gasifier and electricity production using solid oxide fuel cells and gas turbines. The use of oxygen to supply the heat necessary for the endothermic carbon – steam reaction requires an additional 34 % moles of carbon per mole of steam. Half a century ago it was suggested that this heat can be supplied by the fuel cells. Such a concept is similar to the megawatt molten carbonate fuel cell power plants commercialized by Fuel Cell Energy, Inc. in which natural gas is internally reformed with steam, with an efficiency of larger than 50 percent and battery life of over one year.

Such a new concept for production of electricity from coal using molten carbonate fuel cells is proposed. It involves feeding fine coal particles with steam into the anode compartment of the fuel cell in which the waste heat from the fuel cell is used to produce synthesis gas which reacts electrochemically. The overall reaction is carbon plus oxygen yields carbon dioxide. Hence the reversible

efficiency of this process is near 100 percent, as in the direct carbon fuel cell. The gaseous product is carbon dioxide with impurities which can be scrubbed to produce carbon dioxide for sequestration. The impurities from coal in the bubbling gasifier-fuel cell, ash and sulfur, can be potentially removed by re-circulating the electrolyte, cleaning the electrodes with pulses of steam and by filtering the electrolyte.

The computed efficiency for power generation is of the order of 70% of the enthalpy of carbon combustion (Gidaspow and Jiradilok, 2007a, 2007b).

- **Mass transfer coefficients**

It was known for half a century that the Sherwood and Nusselt numbers in fluidized beds are often three orders of magnitude lower than the classical diffusion controlled limit of two. We have shown (Chalermsinsuwan et al., 2008a, 2008b) that our kinetic theory based computer codes correctly compute low Sherwood numbers in agreement with published experimental data. For tall fluidized bed risers the computed behavior is similar to that for convective diffusion in a channel, but with a greatly reduced mass transfer. The Sherwood numbers are low due to formation of clusters, consistent with our measurements of granular temperature.

We measured the mass transfer coefficients with ozone decomposition in our two dimensional bubbling fluidized bed and the free board in which there was a visible formation of clusters. From the data in a free board we obtained the reaction rate constant for ozone decomposition. This number is in reasonable agreement with literature values. Using this reaction rate constant and measured concentration profiles in the bubbling bed, we determined the mass transfer coefficient. The resistance due to mass transfer in a bubbling bed was very significant. The Sherwood number based on the bubble diameter is of the order of one. However, the Sherwood number based on the particle diameter is very

low, consistent with measurements in the literature. Our multiphase CDF computer code predicts such behavior.

PUBLICATIONS PARTIALLY SPONSORED BY THIS PROJECT

1. Jiradilok, V., D. Gidaspow, and R.W. Breault, “Computation of gas of solids dispersion coefficients in turbulent risers and bubbling beds,” Chemical Engineering Science 62 (2007) 3397-3409

Abstract

A literature review shows that dispersion coefficients in fluidized beds differ by more than five orders of magnitude. To understand the phenomena, two types of hydrodynamics models which compute turbulent and bubbling behavior were used to estimate radial and axial gas and solids dispersion coefficients. The autocorrelation technique was used to compute the dispersion coefficients from the respective computed turbulent gas and particle velocities.

The computations show that the gas and the solids dispersion coefficients are close to each other in agreement with measurements. The simulations show that the radial dispersion coefficients in the riser are two to three orders of magnitude lower that the axial dispersion coefficients, but less than an order of magnitude lower for the bubbling bed at atmospheric pressure. The dispersion coefficients for the bubbling bed at 25 atmospheres are much higher than at atmospheric pressure due to the high bed expansion with smaller bubbles.

The computed dispersion coefficients are in reasonable agreement with the experimental measurements reported over the last half century.

2. Gidaspow, D. and V. Jiradilok, “Nanoparticle gasifier fuel cell for sustainable energy future,” Journal of Power Sources 166 (2007a) 400-410

Abstract

A new concept for production of electricity from biomass or coal using molten carbonate fuel cells is proposed. It involves feeding fine coal particles or biomass, for sustainable energy future, with steam into the anode compartment

of the fuel cell in which the waste heat from the fuel cell is used to produce synthesis gas which reacts electrochemically. This concept is illustrated using carbon nanoparticles as the fuel.

A computational fluid dynamics (CFD) model for the gasifier-fuel cell has been developed. Concentration, temperature and current density profiles have been computed. The computations show that practical current densities can be achieved. However, for the new concept to work well the carbon monoxide produced by the gasification should be allowed to react electrochemically. The computed temperature distributions for adiabatic operation show an initial drop in temperature due to gasification, followed by a rise which will have to be balanced by staggering the cells or by other means using the CFD design method.

3. Jiradilok, V., D. Gidaspow, R.W. Breault, L.J. Shadle, C. Gunther, and S. Shi, “Computation of turbulence and dispersion of cork in the NETL riser”, Chemical Engineering Science 63 (2008) 2135-2148

Abstract

The knowledge of dispersion coefficients is essential for reliable design of gasifiers. However, a literature review had shown that dispersion coefficients in fluidized beds differ by more than five orders of magnitude. This study presents a comparison of the computed axial solids dispersion coefficients for cork particles to the NETL Morgantown riser cork data. The turbulence properties, the Reynolds stresses, the kinetic energy spectra and the radial and axial gas and solids dispersion coefficients are computed.

The standard kinetic theory model described in Gidaspow’s 1994 book, Multiphase Flow and Fluidization, Academic Press and available in the M-FIX and commercial codes e.g. FLUENT, was used to compute the measured axial solids volume fraction profiles for flow of cork particles in the Morgantown riser. The Johnson-Jackson boundary conditions were used. The standard drag correlation was used, without modification. This study shows that the computed solid volume fractions for the low flux flow are within the experimental error of

those measured. At higher solid fluxes the simulated solids volume fractions are close to the experimental measurements, but deviate significantly at the top of the riser. This disagreement may be due to use of simplified geometry in the simulation and over-prediction of the experimental volume fractions due to their computation from the grossly simplified pressure drop equals to the weight of the bed expression.

This study concludes that the axial and radial gas and solids dispersion coefficients in risers operating in the turbulent flow regime can be computed using a good multiphase computational fluid dynamics model.

4. Gidaspow, D. and V. Jiradilok, “Efficient Coal Gasifier-Fuel Cell with CO2 Sequestration,” The Clearwater Coal Conference, The 32nd International Technical Conference on Coal Utilization & Fuel Systems, Clearwater, Florida, U.S.A. June 13, 2007b

Abstract

A new concept for production of electricity from coal using molten carbonate fuel cells is proposed. It involves feeding 200 mesh coal particles with steam into the anode compartment of the fuel cell in which the waste heat from the fuel cell is used to produce synthesis gas which reacts electrochemically. The overall reaction is carbon plus oxygen yields carbon dioxide. Hence the reversible efficiency of this process is near 100 per cent, as in the direct carbon fuel cell. The gaseous product is carbon dioxide with impurities which can be scrubbed to produce carbon dioxide for sequestration. The impurities from coal in the bubbling gasifier-fuel cell, ash and sulfur, can be potentially removed by re-circulating the electrolyte, cleaning the electrodes with pulses of steam and by filtering the electrolyte.

A kinetic theory based computational fluid dynamics (CFD) model for a bubbling bed gasifier-fuel cell has been developed. Concentration, temperature and current density profiles have been computed. The computed efficiency for power generation is of the order of 70% of the enthalpy of carbon combustion.

5. Chalermsinsuwan, B., P. Piumsomboon, and D. Gidaspow, “Kinetic theory based computation of PSRI riser- Part I: Estimate of mass transfer coefficient”, available online in Chemical Engineering Science, 2008a

Abstract

The PSRI benchmark challenge problem one is modeled using kinetic theory based CFD with the EMMS drag law. These computations give a better comparison than the previous models to measured solids mass flux, solids density and pressure drop.

The computer model was also used to calculate axial and radial normal Reynolds stresses, energy spectra, power spectra, granular temperatures, the FCC viscosity and axial and radial dispersion coefficients. The computed cluster sizes agreed with the published empirical correlations. Then, the mass transfer coefficients and the Sherwood numbers are estimated based on particle cluster sizes. The conventional Sherwood number is scaled with the particle cluster diameter. The Sherwood number is the order of 10^{-2} and the mass transfer coefficient is the order of 10^{-3} m/s. This Sherwood number is two orders of magnitude smaller than the diffusion controlled limit of two based on particle diameter, in agreement with the experimental data for fluidization of fine particles.

6. Chalermsinsuwan, B., P. Piumsomboon, and D. Gidaspow, “Kinetic theory based computation of PSRI riser- Part II: Computation of mass transfer coefficient with chemical reaction”, available online in Chemical Engineering Science, 2008b

Abstract

The design of circulating fluidized bed systems requires the knowledge of mass transfer coefficients or Sherwood numbers. A literature review shows that these parameters in fluidized beds differ up to seven orders of magnitude.

To understand the phenomena, a kinetic theory based computation was used to simulate the PSRI challenge problem I data for flow of FCC particles in a

riser, with an addition of an ozone decomposition reaction. The mass transfer coefficients and the Sherwood numbers were computed using the concept of additive resistances. The Sherwood number is of the order of 4×10^{-3} and the mass transfer coefficient is of the order of 2×10^{-3} m/s, in agreement with the measured data for fluidization of small particles and the estimated values from the particle cluster diameter in part one of this paper. The Sherwood number is high near the inlet section, then decreases to a constant value with the height of the riser. The Sherwood number also varies slightly with the reaction rate constant. The conventionally computed Sherwood number measures the radial distribution of concentration caused by the fluidized bed hydrodynamics, not the diffusional resistance between the bulk and the particle surface concentration. Hence, the extremely low literature Sherwood numbers for fluidization of fine particles do not necessarily imply very poor mass transfer.

7. Kashyap, M. and Gidaspow, D, "Measurement of mass transfer coefficients in a bubbling bed with ozone decomposition", Paper in preparation, Extended Abstract in November 2008 Philadelphia AIChE Meeting, Available on CD-ROM

Abstract

We measured the mass transfer coefficients with ozone decomposition in our two dimensional bubbling fluidized bed and the free board in which there was a visible formation of clusters. From the data in a free board we obtained the reaction rate constant for ozone decomposition. This number is in reasonable agreement with literature values. Using this reaction rate constant and measured concentration profiles in the bubbling bed, we determined the mass transfer coefficient. The resistance due to mass transfer in a bubbling bed was very significant. The Sherwood number based on the bubble diameter is of the order of one. However, the Sherwood number based on the particle diameter is very low, consistent with measurements in the literature. Our multiphase CDF computer code predicts such behavior.

STUDENTS

Ph.D. candidates: Mayank Kashyap and Benjapon Chalermsinsuwan, supported by the Thailand Research Fund through the Royal Golden Jubilee Ph.D. Program (Grant No. PHD/0021/2550).

CONCLUSIONS

We have shown that the kinetic theory based CFD codes correctly compute:

(3) Dispersion coefficients

(4) Mass transfer coefficients

Hence, the kinetic theory based CFD codes can be used for fluidized bed reactor design without any such inputs

Computation and measurements of mass transfer and dispersion coefficients in fluidized beds

Mayank Kashyap and Dimitri Gidaspow*
Department of Chemical and Biological Engineering,
Illinois Institute of Technology,
Chicago, IL 60616

Presented at the 2009 NETL Workshop on Multiphase Flow Science,

in Morgantown, WV,

on April 23, 2009

Introduction

Conventional design of circulating fluidized beds, such as gasifiers (Yoon et al., 1978), requires the knowledge of dispersion and mass transfer coefficients or Sherwood numbers. However, these are known to vary by five or more orders of magnitude (Breault, 2006).

We have recently shown that the particle and the gas axial and radial dispersion coefficients (Jiradilok et al., 2007, 2008), and the mass transfer coefficients (Chalermsinsuwan et al., 2009 a,b) can be computed using the kinetic theory based multiphase model, which is available in a commercial FLUENT code, the publically available MFIX (Syamlal, 1998) and in the IIT code (Gidaspow and Jiradilok, 2009).

Hydrodynamic model

The hydrodynamic model for the multiphase flow is based on the generalization of Navier-Stokes equations. The model numerically solved the set of governing conservation equations, mass, momentum, energy and species mass conservation, using the kinetic theory of granular flow (Gidaspow, 1994). The dense phase drag law was based on the Ergun equation, and the dilute drag law was a modification of Wen and Yu drag law (Yang et al., 2003, 2004). However, to model the turbulent fluidization regime, the drag law was modified using the energy minimization principle (Yang et al., 2004). Table 1 summarizes the kinetic theory based model.

Figure 1 shows that the dilute and the dense solids volume fractions of fluid cracking catalyst (FCC) particles can be computed using the modified drag model. We have conducted a similar study to that of Wei et al. (1998 a) in the IIT two-story riser shown in Figure 2. To obtain high fluxes, we have fluidized the downcomer. Figure 3 shows our experimental data for FCC particles plotted on Matsen's phase diagram. Matsen's model is essentially the drift flux model reviewed by Gidaspow (1994). Recently, Gao et al. (2009) also computed the two different volume fractions in the turbulent flow regime using the kinetic theory model in FLUENT, and compared the computations to experiments.

Figure 4 shows that the model is able to resolve the spectral distribution of turbulence, beginning with the low frequency gravity wave down to the high frequency Kolmogorov regime.

We have also simulated flow of cork particles in the NETL riser shown in Figure 5. Figure 6 shows that the pressure profile in the NETL riser with flow of cork is almost identical to the pressure distribution in the PRSI riser for flow of FCC particles when scaled with the density of the particles.

Computation of dispersion coefficients

Figure 7 shows a comparison of the computed axial gas dispersion coefficient to literature correlations. Figure 8 shows a similar computation for the radial gas dispersion coefficients. The radial gas dispersion coefficient is several orders of magnitude lower than the axial dispersion coefficient, as is well known in literature. Figure 9 shows a comparison of the measured NETL cork axial solids dispersion coefficients to the CFD computation and the literature values. Figure 10 shows a comparison of the computed radial solids dispersion coefficients for the cork particles to related measurements in the literature. The gas and the particle dispersion coefficients are close to each other. They are all local values. They vary with axial and radial positions. We have shown that the kinetic theory based hydrodynamic model is capable of computing all the dispersion coefficients with a reasonable comparison to the literature reported in the last half a century.

Measurement of dispersion coefficients in the IIT two-dimensional CFB

Experimental setup

A two-dimensional circulating fluidized bed (CFB) was constructed and modified at IIT, for the measurements of dispersion and mass transfer coefficients, with partial financial support from UOP and the U.S. Department of Energy.

Schematic diagram

Figure 11 shows the schematic diagram of the two-dimensional circulating fluidized bed (CFB) at IIT. The inner walls of the riser section of the fluidized bed were constructed of 0.5 inch thick glass sheets to avoid sticking of FCC particles to the walls, due to electrostatics caused by abrasion. The inside dimensions of the fluidized bed were 2 inch depth by 12 inch width by 50.5 inch height. The glass section was enclosed within a 0.5 inch thick acrylic sheet framework. The downcomer section of the fluidized bed was fabricated of 0.5 inch thick acrylic sheets, with the inside dimensions as 2 inch depth by 12 inch width by 55 inch height. Fine 304 L stainless steel wire support grids (165 x 1400 mesh) were used at the bases of the riser and downcomer sections of the two-dimensional fluidized bed, to support the bed of 75 μm FCC particles. To allow uniform distribution of air at the inlet, two 12.5 and 18.5 inch tall gas distributors were placed below the support grids in the riser and the downcomer sections, respectively. The riser and the downcomer sections were 11 inch apart, horizontally. An acrylic cuboid connector with 3 inch high openings on each side, was placed at an angle of 30 degrees with the horizontal, to connect the riser and the downcomer sections at 3 inches above the distributors. The top sections of

the riser and the downcomer were connected by an acrylic cuboid connector, with 6 inch high openings on each side.

Compressed air was conditioned before entering the fluidized bed. First, a heating coil was used around the inlet gas pipe in an attempt to dry any moisture from the air. Then, the air was flown through a silica gel bed to remove more water from the air stream, before entering another water filter installed in the pipe line. Next, the air pressure was reduced to 30 psig by a pressure regulator. Finally, the air flow rate to the fluidized bed was regulated by directing the air stream through a rotameter with a manual valve. The air entered the distributor of the fluidized bed in the center. Air from the downcomer section of the fluidized bed was discharged to the atmosphere.

Figure 12 shows a photograph of the circulation of 75 μm FCC particles at a low velocity. At the bottom of the riser, there is a formation of bubbles free of particles, not visible in the picture. Figure 13 shows the cluster formation and a typical bubble.

Figure 14 shows the particle image velocimetry (PIV) system, fully described in the paper by Tartan and Gidaspow (2004). Figure 15 shows typical streaks. Table 2 summarizes the system properties for the measurement of dispersion coefficients in the IIT two-dimensional fluidized bed. Figure 16 shows the instantaneous axial and radial velocities. Table 3 presents the measured laminar

and turbulent granular temperatures at the low gas velocity. The granular temperature due to oscillation of particles is much larger than the turbulent oscillations in a low flow rate cluster regime. Hence, mixing is on the level of particles, rather than on the level of clusters.

Figure 17 shows a comparison of the granular temperature in the IIT two-dimensional circulating fluidized bed to the literature values. The measured granular temperature is in agreement with literature values at the low gas velocities in Figure 17. The granular temperature of 10 nm nanoparticles is several orders of magnitude higher than that for micron size particles, at same gas velocities. This high granular temperature of the nanoparticles is due to their random motion caused by collision with air molecules, rather than just caused by shear, as is the case in ordinary granular flow. Appendix A provides a more complete explanation.

Table 4 shows the measured axial and radial dispersion coefficients. Again, the laminar type axial and radial solid dispersion coefficients are bigger than the turbulent type dispersion coefficients. Figure 18 shows a comparison of the measured axial solids dispersion coefficients in the two-dimensional CFB to the literature values. The measured axial dispersion coefficients are low because the measurements were done close to the wall. We had seen this effect in our CFD calculations. Hence, Figure 18 illustrates the local nature of the dispersion

coefficients. Figure 19 shows a similar behavior for the radial solids dispersion coefficients.

Computation of mass transfer coefficients

Chalermsinsuwan et al. (2009 a) modeled the PSRI benchmark challenge problem one using a kinetic theory based CFD model, with the energy minimization multi-scale (EMMS) drag law, without considering reaction. Figure 20 shows a schematic diagram of the circulating fluidized bed test unit for the Fluidization VII benchmark test. They computed clusters of the order of 10^{-2} m, which were then used to estimate the Sherwood numbers and the mass transfer coefficients of the order of 10^{-2} (---) and 10^{-3} m/s, respectively. The Sherwood numbers were two orders of magnitude smaller than the diffusion controlled limit of two based on particle diameter.

The PSRI benckmark challenge problem one for the flow of FCC particles, with the ozone decomposition reaction, was modeled by Chalermsinsuwan et al. (2009 b). Figure 21 shows the effect of the riser height on the computed Sherwood numbers and the mass transfer coefficients for different reaction rate constants. The Sherwood numbers of the order of 4×10^{-3} and the mass transfer coefficients of the order of 2×10^{-3} m/s, were computed using the concept of additive resistances. The Sherwood number was highest at the bottom of the reactor, and decreased with the increase in height before attaining a constant

value. These results showed a similar trend as that experimentally obtained by Kato et al. (1970).

Measurement of mass transfer coefficients in the IIT two-dimensional fluidized bed

Ozone decomposition reaction

Many authors (Fryer and Potter, 1976; Syamlal and O'Brien, 2003) have shown that the ozone reaction is one of the most frequently used chemical reactions for studying reactions in the fluidized bed systems. As described earlier, the computational work using the ozone decomposition reaction in a circulating fluidized bed was recently published by Chalermsinsuwan et al. (2009 b). The ozone decomposition reaction is selected in this study for the measurement of the mass transfer coefficients in the IIT two-dimensional fluidized bed.

Differential reactor system

Figure 22 shows the modified IIT two-dimensional fluidized bed described in Figure 11, for the measurement of the mass transfer coefficients, with ozone decomposition. Table 2 summarizes the system properties for the measurement of the mass transfer coefficients in the IIT two-dimensional fluidized bed. A differential reactor system was used, with eight holes fitted with PVC barbed ball valves at the center of the front face of the riser section, along the "axial or y-direction". The valves were fitted by cautiously drilling the glass and acrylic walls of the riser section of the fluidized bed, using a drill bit specially used for glass.

The purpose of installing the valves was to withdraw time averaged samples of the mixture of ozone and air for further analysis. Small Teflon tubes were connected to the inside openings of each barbed ball valve to withdraw gas samples from the center of the fluidized bed, along the “radially inward or z-direction”. Two more valves were fitted at the bottom and the top of the riser section of the fluidized bed to mix the ozone gas to the fluidizing air supply and to withdraw the samples of the mixture of gases from the top, respectively. Figure 23 shows a photograph of the fluidized bed system with barbed ball valves.

Apparatuses for the ozone decomposition reaction

After doing intensive survey, the ozone generator and the ozone analyzer were purchased from Ozone Solutions, Inc. Figure 24 shows the ozone generator used in this study. The ozone generator, HG-1500, with variable output control, had a capacity to generate 750 mg/hr of ozone on dry air, and 1500 mg/hr of ozone on oxygen. The gas used in this study was dry air. Corona discharge method was the principle for the generation of ozone in this system.

The temperature and humidity of the air and the ozone gas mixture in the fluidized bed were measured with standard digital temperature and humidity meters, respectively.

Figure 25 shows the ozone analyzer used to measure the concentration of ozone in the fluidized bed system. The ozone analyzer, UV-100, was used to measure

the ozone concentrations at the inlet, outlet and eight other positions along the "axial or y-direction" in the fluidized bed.

Preparation of catalyst

Dhandapani and Oyama (1997) reviewed in Applied Catalysis B: Environmental that the noble metals and the metal oxides are the active catalysts for the ozone decomposition reaction. Due to the high cost of noble metals, the metal oxide catalysts are commonly used for the ozone decomposition.

The literature survey showed that some of the catalysts used by authors, for the ozone decomposition reaction in fluidized beds, are: FCC particles coated with ferric nitrate (Fan et al., 2008); FCC particles impregnated with ferric oxide (Jiang et al., 1991); sand particles impregnated with ferric oxide (Fryer and Potter, 1976); and γ-alumina particles impregnated with ferric oxide (Pagliolico et al., 1992).

The catalysts used in this study were FCC particles impregnated with ferric nitrate. The FCC particles, which are mainly composed of porous amorphous aluminum hydro-silicate, were activated by soaking them overnight in a 5 wt% solution of ferric nitrate purchased from Sigma-Aldrich. The FCC particles were then dried and calcined in an oven at 475^0C for 2-3 hours, until no further NO_2 was released from ferric nitrate. The ferric nitrate was converted to ferric oxide, which was the active component for the ozone decomposition reaction:

$$Fe(NO_3)_3.nH_2O \xrightarrow{475^0C} \frac{1}{2}Fe_2O_3 + 3NO_2 + \frac{3}{4}O_2 + nH_2O$$

Experimental procedure for the measurement of mass transfer coefficients

Ozone concentration measurements

The ozone analyzer shown in Figure 25 was warmed for about an hour before performing experiments. A weighed sample of the ferric oxide coated FCC particles was added to the two-dimensional fluidized bed. Initial height of the bed was noted. For the mass transfer experiments, the downcomer side of the circulating fluidized bed was blocked to fluidize the system as a bubbling bed. The air flow was set to fluidize the bed in the bubbling fluidization regime. Two previously calibrated rotameters were used to control the flow rates of the air entering the fluidized bed system. One rotameter was used to fluidize the bed, whereas, the other was used to introduce very low amount of air to the ozone generator described above. The oxygen from the air was converted to ozone in the ozone generator. The ozone was then mixed with the fluidizing air in the distributor of the fluidized bed. The concentration of ozone in the fluidizing air entering the fluidized bed was measured by taking samples of air from the distributor, by opening the PVC barbed ball valve connected to the ozone analyzer. The initial ozone concentration was fixed around 13 PPM throughout the experiments performed at a superficial gas velocity of 34.34 cm/s.

The expanded bed height was noted. To measure the ozone concentrations at different levels along the “axial or y-direction” in the fluidized bed, each one of the

eight PVC barbed ball valves were opened individually. The samples of the mixture of air and ozone gases were withdrawn from the fluidized bed at various vertical levels, moving up from the bottom, each time for about 1 minute after waiting for 5 minutes, for the measurements of ozone concentrations by the ozone analyzer.

Light diode assembly to measure the solids volume fractions

The light diode assemblies have been successfully used to understand the dynamics of fluidized beds. The technique of using a light diode assembly to measure the solid concentrations is well known (Driscoll, 2007; Driscoll and Gidaspow, 2007; Kashyap et al., 2008; Kashyap, 2009).

The solids volume fractions were measured at different levels along the “axial or y-direction” in the fluidized bed, using a light diode assembly. The solids volume fractions at each position were averaged three times, each time averaged for around 20 seconds.

Results and discussion

Ozone concentration

Figure 26 shows the axial variation of the ozone concentration in the circulating fluidized bed reactor, at a superficial gas velocity of 34.34 cm/s. The concentration of ozone decreased upon moving up in the reactor due to the successive conversion caused by the reaction on the surface of catalysts.

Dimensionless form of the axial variation of the ozone concentration, i.e. the ratio of local to inlet ozone concentrations, is shown in Figure 27.

Solids volume fraction

Figure 28 shows the axial variation of the solids volume fractions measured in the circulating fluidized bed, using the light diode assembly described earlier.

Calculation of Mass transfer coefficients and Sherwood numbers

The primary information needed for the chemical reactions is the reaction rate constant. The literature survey shows that the experimentally obtained reaction rate constants for the first order ozone decomposition reaction, vary by three orders of magnitude. In this study, the rate of reaction was obtained from the ozone concentration measurements in the fluidized bed.

Chalermsinsuwan et al. (2009 b) showed that the conservation of species equation gives the one dimensional steady state balance as:

$$v_y \varepsilon_g \frac{dC_{O_3}}{dY} = r_i \qquad (1)$$

where, v_y is the velocity of gas phase in axial or vertical direction, Y is the axial or vertical distance and C_{O_3} is the ozone mass or molar concentration.

Since the decomposition of ozone is a first order reaction, the reaction rate constant is independent of the gas concentration, and can be written as:

$$\text{Rate of ozone decompostion reaction} = \mathrm{r_{O_3}} = -\mathrm{k_{reaction}} \mathrm{C_{O_3}} \varepsilon_s \quad (2)$$

where, $k_{reaction}$ is the reaction rate constant, C_{O_3} is the ozone concentration and ε_s is the solids volume fraction or particle concentration of catalyst used in the reaction.

Substitution of the rate of reaction in the one dimensional steady state balance equation gives:

$$\mathrm{v_y} \varepsilon_g \frac{\mathrm{dC_{O_3}}}{\mathrm{dY}} = -\mathrm{K C_{O_3}} \varepsilon_s \quad (3)$$

where, K is the effective rate constant.

Chalermsinsuwan et al. (2009 b) showed that the overall resistance gives the mass transfer coefficient as follows:

$$\frac{1}{K} = \frac{1}{k_{mass\ transfer} a_v} + \frac{1}{k_{reaction}} \quad (4)$$

The Sherwood number (Sh) is then given by the equation (5) given below:

$$Sh = \frac{k_{mass\ transfer} d_p}{D} \quad (5)$$

where, d_p is the diameter of the catalyst particle and D is the molecular diffusivity equal to 2.88 x 10^{-5} m^2/s.

Results and discussion

For the differential reactor, C_{O_3} and ε_s were the average concentrations of ozone and catalyst, respectively, taken between pairs of two consecutive points along the "axial or y-direction", at a distance of Y. The product of the gas velocity, v_g, and the volume fraction of gas phase, ε_g, can be represented as the superficial gas velocity, U_g (Gidaspow, 1994). Values of the solids volume fractions were obtained from the data presented in Figure 28. The substitution of all the parameters in equation 3 gave the effective rate constant, K, between the pairs of two consecutive points along the "axial or y-direction" direction. Figure 29 presents the axial variation of the effective rate constant, K, in the two-dimensional bed. It can be seen clearly that the effective rate constant is a local property.

To obtain the reaction rate constant, $k_{reaction}$, the effective rate constant, K, was equated to the reaction rate constant, in the free board regime. The values of the reaction rate constants are shown in Table 5. In the literature, the values of the reaction rate constants for the ozone decomposition reaction on the surface of catalyst coated FCC particles are found to vary by three orders of magnitude (Chalermsinsuwan et al., 2009 b; Ouyang et al., 1993, 1995; Jiang et al., 1991). The difference in the values of the reaction rate constants for the first order ozone decomposition reactions is due to different activities of catalysts, and the temperature and humidity conditions during the experiments. Our values of the reaction rate constants of 6.95-9.88 s^{-1} are in reasonable agreement with those obtained by other authors.

Measurement of Sherwood number and mass transfer coefficient

The mass transfer coefficients and the Sherwood number were calculated using equations 4 and 5, respectively. Table 6 summarizes the measured Sherwood numbers and the mass transfer coefficients in the bubbling and cluster regions of the circulating fluidized bed, with various reaction rate constants shown in Table 5. The mass transfer coefficients and the Sherwood numbers in the bubbling and the cluster regions of the circulating fluidized bed are of the order of 10^{-5} and 10^{-4}, respectively. As shown by Chalermsinsuwan et al. (2009 b), the Sherwood number is low due to its representation in terms of the particle diameter or surface area per unit volume, a_v. Equation 5 can be rewritten as:

$$Sh = \frac{k_{mass\ transfer} d_p}{D} = \frac{6 k_{mass\ transfer}}{a_v D} \qquad (6)$$

The equation shows that for large a_v of small particles, the mass transfer coefficient must be extremely high to give a Sherwood number of two. The formation of clusters significantly decreases the mass transfer coefficients and the Sherwood numbers.

Figure 30 shows that the values of the Sherwood number lie in the lower Reynolds number ($\mathrm{Re_k} = \frac{\rho_g d_p U_g}{\mu_g} \approx 1.57$) region of the compared Sherwood numbers by Breault et al. (2009). The figure shows that the Sherwood number is a local quantity that changes with the axial position in the fluidized bed.

As mentioned earlier, Figure 13 shows the formation of bubbles and clusters in the circulating fluidized bed. The largest cluster in the free board regime was of the order of 14 cm long, whereas, the largest bubble in the bubbling region was of the order of 11 cm in diameter. Table 6 shows that the substitution of cluster and bubble diameters instead of particle diameter in the equation of Sherwood number, $Sh_{cluster} = \frac{Sh_{particle} d_{cluster}}{d_{particle}}$ or $Sh_{bubble} = \frac{Sh_{particle} d_{bubble}}{d_{particle}}$, gives Sherwood numbers for clusters in the free board regime and for bubbles in the bubbling regime of the orders 0.2 and 1.5, respectively. Also, for the diffusion limit of 2 for the Sherwood numbers, the estimated cluster and bubble diameters are shown in Table 6. The table shows that the Sherwood numbers based on the particle size are much smaller than those based on the cluster or the bubble sizes. This also deduces that the convection to diffusion ratio for fine particles is lower than that for large particles.

Computational fluid dynamics (CFD) simulations using the ozone decomposition reaction in the circulating fluidized bed used in this study are underway. A kinetic theory based model, with the EMMS drag, is being used in the commercial software, FLUENT (Fluent, 2005 b). The user-define function (UDF) codes (Fluent Inc., 2005 a) for the EMMS drag and the ozone decomposition reaction, written in C programming language using Microsoft Visual C++, were incorporated in FLUENT. In reality, the bubbles in the circulating fluidized bed do not contain almost any particles. Hence, there is negligible conversion of ozone

inside the bubbles. To avoid the computation of reaction inside the bubbles, the clusters or bubbles need to be resolved properly. Also, in reality, there is a bypassing of gas in the center of the fluidized bed of FCC particles, along the “radial or z-direction”, due to lower concentrations of solids as compared to that near the walls. Hence, extremely fine grids in a three-dimensional model are being used in performing simulations. The inability to resolve the clusters could result in the mismatching of the ozone concentrations along the “axial or y-direction” in the fluidized bed.

Conclusions

We have shown that the kinetic theory based CFD codes, such as the commercial code FLUENT, the publically available MFIX code developed at the Department of Energy, National Energy Technology Laboratory, and the IIT code fully described in the three volume book, “Computational Techniques”, by Gidaspow and Jiradilok (2009), correctly compute:

1. Dispersion coefficients
2. Mass transfer coefficients

Hence, the kinetic theory based CFD codes can be used for fluidized bed reactor design without any such inputs.

Symbols

a_v = external surface per volume of catalyst, m^{-1}

$\langle C \rangle$ = mean velocity, m/s

c_p = heat capacity at constant pressure, J/(kg-K)

C_{O_3} = molar concentration of ozone, $kgmol/m^3$

$C_{O_3(inlet)}$ = inlet molar concentration of ozone, $kgmol/m^3$

C_d = drag coefficient, dimensionless

d_{bubble} = particle bubble diameter, m

$d_{cluster}$ = particle cluster diameter, m

d_p = catalyst particle diameter, m

$d_{particle}$ = catalyst particle diameter, m

D = molecular diffusivity, m^2/s

e = restitution coefficient between particles, dimensionless

e_w = restitution coefficient between particle and wall, dimensionless

g = gravity force, kg/m^3

g_0 = radial distribution function, dimensionless

H = height of fluidized bed, m

h = specific enthalpy, J/kg

I = unit tensor, dimensionless

k = Boltzmann constant, J/K

$k_{mass\ transfer}$ = mass transfer coefficient, m/s

$k_{reaction}$ = reaction rate constant, s^{-1}

K = effective rate constant, m/s

m = mass of nanoparticles, kg

n = stoichiometric coefficient, dimensionless

n = unit vector, dimensionless

p = pressure, Pa

P_s = solids pressure, Pa

Q_{gs} = intensity of heat exchange from gas phase to solid phase, J/(s-m^3)

Q_{sg} = intensity of heat exchange from solid phase to gas phase, J/(s-m^3)

r = reaction rate, kgmol/(s-m^3)

r_i = reaction rate of specie "*i*", kgmol/(s-m^3)

Re_k = Reynolds number, dimensionless

S = source term (e.g., due to chemical reaction), J/(s-m^3)

Sh = Sherwood number based on particle diameter, dimensionless

Sh_{bubble} = Sherwood number based on particle bubble diameter, dimensionless

$Sh_{cluster}$ = Sherwood number based on particle cluster diameter, dimensionless

t = time, s

T = temperature, K

U_g = superficial gas velocity, m/s

v = *phase velocity, m/s*

$v_{s,\,slip}$ = slip velocity of particle at the wall, m/s

$v_{s,\,w}$ = tangential velocity of particle at the wall, m/s

W_s = solids flux, kg/(m^2-s)

x = radial distance from center of fluidized bed, m

y = axial distance from bottom of fluidized bed, m

z = radially inward distance from the front wall, m

y_i = mass fraction of specie "*i*", dimensionless

Y = axial or vertical distance, m

Greek letters

β_{gs} = gas–particle interphase drag coefficient, kg/(s-m^3)

γ_s = collisional dissipation of solid fluctuating energy, kg/(m-s^3)

γ_w = collisional dissipation of solid fluctuating energy at the wall, kg/(m-s^3)

ε = void fraction, dimensionless

ε_s = solids volume fraction, dimensionless

$\varepsilon_{s,avg}$ = average solids volume fraction, dimensionless

$\varepsilon_{s,max}$ = solids volume fraction at maximum packing, dimensionless

θ = granular temperature, m^2/s^2

θ_w = granular temperature at the wall, m^2/s^2

κ_s = conductivity of the fluctuating energy, kg/(m-s)

μ = viscosity, kg/m s

ξ = bulk viscosity, kg/(m-s)

ρ = density, kg/m^3

σ = solids stress, N/m^2

τ = stress tensor, Pa

ϕ = specularity coefficient, dimensionless

Subscripts

g = gas phase

nano. = nanoparticles

O_3 = ozone specie

s = solid phase

y = axial direction

0 = initial condition

Acknowledgement

The authors would like to acknowledge the financial support for this study by the US Department of Energy University Grant (DE-FG26-06NT42736). We thank Dr. Ronald Breault for discussion and interaction with us during the course of the project.

References

1. R.W. Breault, A review of gas–solid dispersion and mass transfer coefficient correlations in circulating fluidized beds. Powder Technology 163 (Issues 1-2) (2006), 9–17.
2. R.W. Breault, C.P. Guenther, L.J. Shadle, Velocity fluctuation interpretation in the near wall region of a dense riser, Powder Technology 182 (2008) 137-145.
3. R.W. Breault, C.P. Guenther, Mass transfer in the core-annular and fast fluidization flow regimes of a CFB, Powder Technology 190 (2009) 385-389.
4. B. Chalermsinsuwan, P. Piumsomboon, D. Gidaspow, Kinetic theory based computation of PSRI riser: Part I—Estimation of mass transfer coefficient, Chemical Engineering Science 64 (2009 a) 1195-1211.
5. B. Chalermsinsuwan, P. Piumsomboon, D. Gidaspow, Kinetic theory based computation of PSRI riser: Part II—Computation of mass transfer coefficient with chemical reaction, Chemical Engineering Science 64 (2009 b) 1212-1222.
6. B. Dhandapani, S.T. Oyama, Gas phase ozone decomposition catalysts, Applied Catalysis B: Environmental 11 (1997) 129-166.
7. M.C. Driscoll, A study of the fluidization of FCC particles and nanoparticles in a rectangular bed and a riser, Ph.D. Thesis, Illinois Institute of Technology, Chicago, Illinois, 2007.

8. M.C. Driscoll, D. Gidaspow, Wave propagation and granular temperature in fluidized beds of nanoparticles, A.I.Ch.E. Journal 53 (2007) 1718.
9. C. Fan, Y. Zhang, X. Bi, W. Song, W. Lin, L. Luo, Evaluation of downer reactor performance by catalytic ozone decomposition, Chemical Engineering Journal 140 (2008) 539-554.
10. Fluent Inc., Fluent 6.2 UDF manual, Fluent Inc., Lebanon, NH. 2005 a.
11. Fluent Inc., Fluent 6.2 user's guide, Fluent Inc., Lebanon, NH, 2005 b.
12. C. Fryer, O.E. Potter, Experimental investigation of models for fluidized bed catalytic reactors, A.I.Ch.E. Journal 22 (1976) 38–47.
13. J. Gao, X. Lan, Y. Fan, J. Chang, G. Wang, C. Lu, C. Xu, CFD modeling and validation of the turbulent fluidized bed of FCC particles, A.I.Ch.E. Journal 55 (2009) 1680-1694.
14. D. Gidaspow, Multiphase flow and fluidization: Continuum and kinetic theory descriptions, Academic Press, New York, 1994.
15. D. Gidaspow, V. Jiradilok, Computational techniques: The multiphase CFD approach to fluidization and green energy technologies (includes CD-ROM), Nova Science Publishers, New York, 2009.
16. P. Jiang, H. Bi, R. Jean, L. Fan, Baffle effects on performance of catalytic circulating fluidized bed reactor, A.I.Ch.E. Journal 37 (1991) 1392–1400.
17. V. Jiradilok, D. Gidaspow, S. Damronglerd, W.J. Koves, R. Mostofi, Kinetic theory based CFD simulation of turbulent fluidization of FCC particles in a riser, Chemical Engineering Science 61 (2006 a) 5544–5559.

18. V. Jiradilok, D. Gidaspow, J. Kalra, S. Damronglerd, S. Nitivattananon, Explosive dissemination and flow of nanoparticles, Powder Technology 164 (2006 b) 33-49.
19. V. Jiradilok, D. Gidaspow, R.W. Breault, Computation of gas and solid dispersion coefficients in turbulent risers and bubbling beds. Chemical Engineering Science 62 (2007) 3397–3409.
20. V. Jiradilok, D. Gidaspow, R.W. Breault, L.J. Shadle, C. Guenther, S. Shi, Computation of turbulence and dispersion of cork in the NETL riser, Chemical Engineering Science 63 (2008) 2135-2148.
21. M. Kashyap, Measurements and computation of dispersion and mass transfer coefficients in fluidized beds, Ph.D. Thesis, Illinois Institute of Technology, Chicago, Illinois, 2009.
22. M. Kashyap, D. Gidaspow, M. Driscoll, Effect of electric field on the hydrodynamics of fluidized nanoparticles, Powder Technology 183 (2008) 441-453.
23. K. Kato, H. Kubota, C.Y. Wen, Mass transfer in fixed and fluidized beds, Chemical Engineering Progress Symposium Series 105 (1970) 87–99.
24. S. Ouyang, J. Lin, O.E. Potter, Ozone decomposition in a 0.254 m diameter circulating fluidized bed reactor, Powder Technology 75 (1993) 73–78.
25. S. Ouyang, J. Lin, O.E. Potter, Circulating fluidized bed as a catalytic reactor: experimental study, A.I.Ch.E. Journal 41 (1995) 1534–1542.

26. S. Pagliolico, M. Tiprigan, G. Rovero, A. Gianetto, Pseudo-homogeneous approach to CFB reactor design, Chemical Engineering Science 47 (1992) 2269–2274.
27. M. Syamlal, MFIX document numerical technique, Department of Energy Report DOE/MC31346-5824, January 1998.
28. M. Syamlal, T.J. O'Brien, 2003. Fluid dynamic simulation of O_3 decomposition in a bubbling fluidized bed, A.I.Ch.E. Journal 49 (2003) 2793–2801.
29. M. Tartan, D. Gidaspow, Measurement of granular temperature and stresses in risers, A.I.Ch.E. Journal 50 (2004) 1760–1775.
30. F. Wei, H. Lin, Y. Cheng, Z. Wang, Y. Jin, Profiles of particle velocity and solids fraction in a high-density riser, Powder Technology 100 (1998 a) 183–189.
31. F. Wei, Y. Cheng, Y. Jin, Z.Q. Yu, Axial and lateral dispersion of fined particles in a binary-solid riser, Canadian Journal of Chemical Engineering 76 (1998 b) 19–26.
32. N. Yang, W. Wang, W. Ge, J. Li, CFD simulation of concurrent-up gas–solid flow in circulating fluidized beds with structure-dependent drag coefficient, Chemical Engineering Journal 96 (2003) 71–80.
33. N. Yang, W. Wang, W. Ge, L. Wang, J. Li, Simulation of heterogeneous structure in a circulating fluidized-bed riser by combining the two-fluid model with the EMMS approach, Industrial and Engineering Chemistry Research 43 (2004) 5548–5561.

34. H. Yoon, J. Wei, M.M. Denn, A model for moving-bed coal gasification reactors, A.I.Ch.E. Journal 24 (1978) 885–903.

Appendix A

In response to the question at the 2009 NETL Workshop by Prof. Fox

Granular temperature for 10 nm fumed silica particles

Batch fluidization of nanoparticles in rectangular fluidized beds was studied at IIT by various authors (Jiradilok et al., 2006 b; Driscoll and Gidaspow, 2007; Kashyap et al., 2008). The solids volume fractions were determined using a light diode assembly.

The fluidization was without bubbles, and the bed expanded almost linearly with inlet gas velocity. The effect of electric field on the hydrodynamics of fluidized nanoparticles was studied by Kashyap et al. (2008), who observed a decrease in the bed height upon the application of electric field. The dependence of particle concentration as a function of height can be explained by a barometric type formula applied to nanoparticles, as given by:

$$\frac{d\sigma}{dx} + g\varepsilon_s(\rho_s - \rho_g) - \beta_{gs} v_g = 0 \qquad (7)$$

where, the drag force balances the solids pressure and the buoyant force.

For dilute solids volume fractions, the solids pressure can be expressed by the following relationship from the kinetic theory of granular flow (Gidaspow, 1994):

$$\sigma = \varepsilon_s \rho_s \theta \qquad (8)$$

where, σ is the solids pressure, ε_s is the solids volume fraction, ρ_s is the density of particles and θ is the granular temperature. Integration of the equation (7) gives the solution as (Driscoll and Gidaspow, 2007):

$$\ln\left[\frac{\varepsilon_{s0}-\varepsilon_{s,avg}}{\varepsilon_{s}-\varepsilon_{s,avg}}\right]=\frac{g}{\theta}x \qquad (9)$$

A plot of the logarithm of the ratio of the solids volume fractions versus the height, x, gives the ratio of the gravity to the granular temperature. The values of the granular temperature for the nanoparticles can be explained due to Brownian motion of the nanoparticles suspended in air by equating the kinetic energy of the air molecules to the kinetic energy of the nanoparticles, as shown below:

$$\frac{3}{2}kT=\frac{1}{2}m_{nano.}\left\langle C^{2}\right\rangle_{nano.} \qquad (10)$$

where, $\frac{\left\langle C^{2}\right\rangle_{nano.}}{2}$ is the random kinetic energy of nanoparticles.

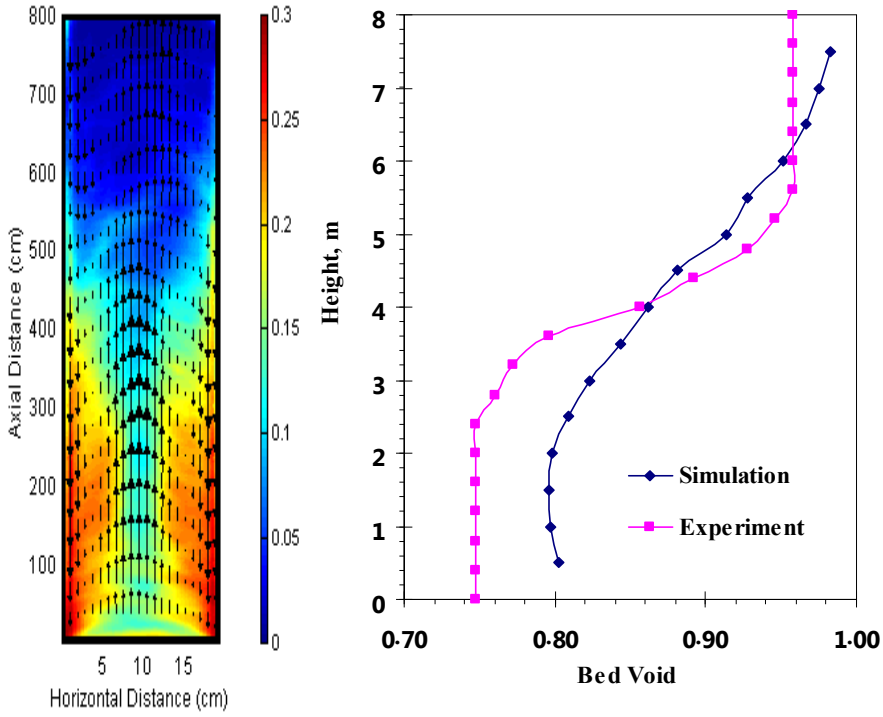

Figure 1. Computed solids volume fraction structure in the Wei et al. (1998 a) riser, showing turbulent flow regime
(Jiradilok et al., 2006 a)

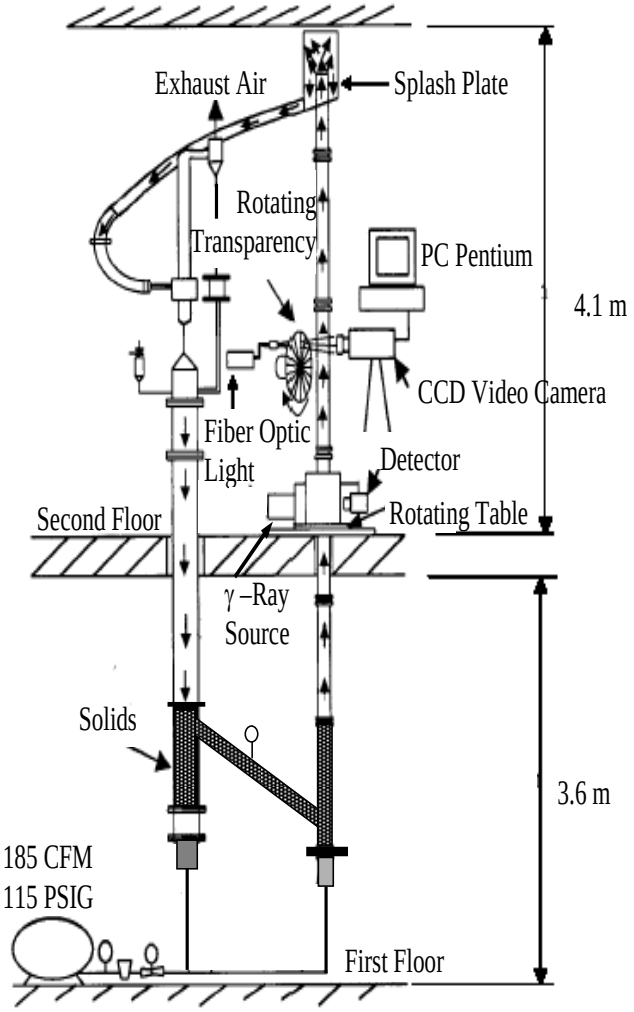

Figure 2. Schematic diagram of the IIT riser with splash plate and fluidized downcomer to obtain high flux
(Kashyap, 2009)

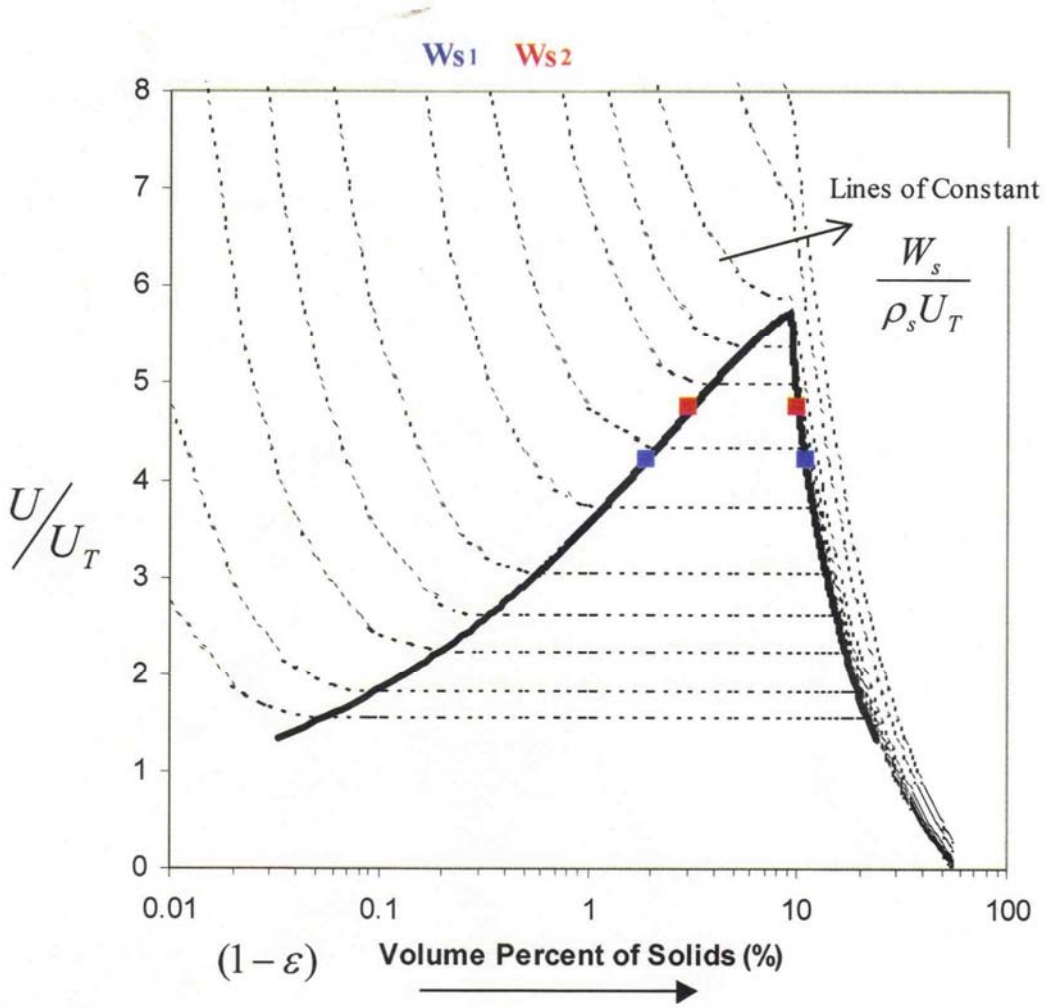

Figure 3. Comparison of experimental data obtained in the IIT riser with Matsen's phase diagram for gas-particle flow; W_{s1} = 13.4 kg/(m^2-s), W_{s2} = 7.58 kg/(m^2-s)

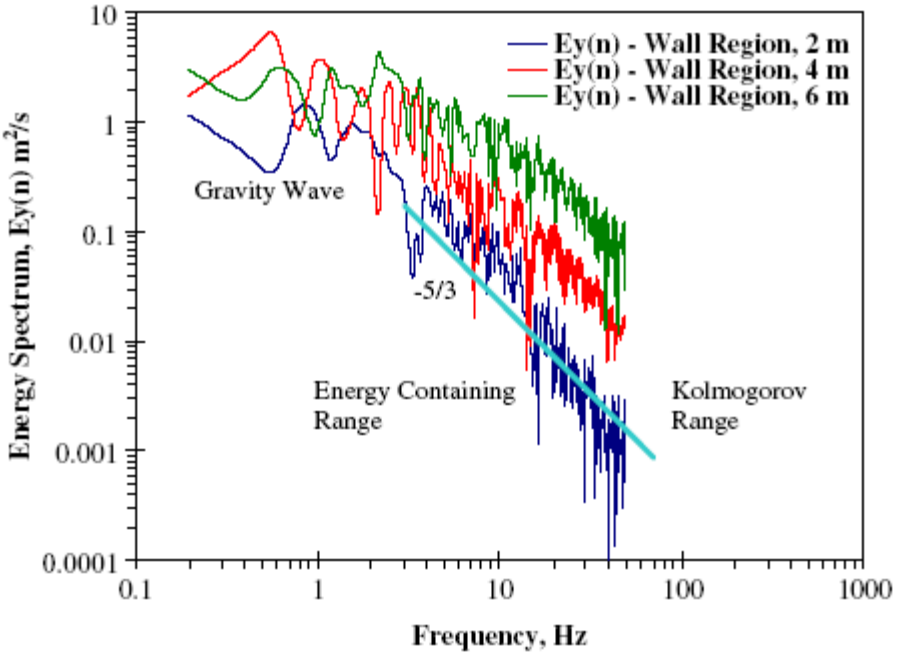

Figure 4. Computed vertical energy spectra in the Wei et al. (1998 a) riser, at various heights for W_S = 98.8kg/m^{2}s and U_g = 3.25 m/s
(Jiradilok et al., 2006 a)

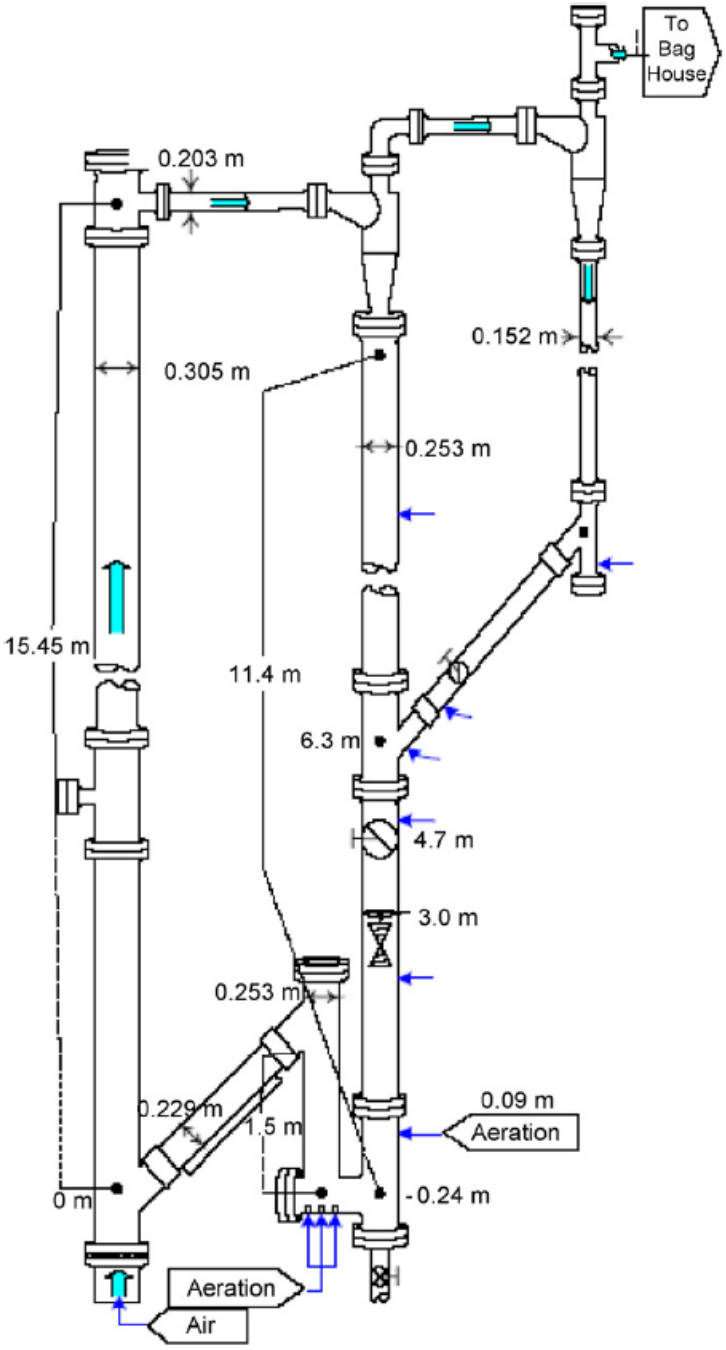

Figure 5. Schematic diagram of the NETL circulating fluidized bed riser (Jiradilok et al., 2008)

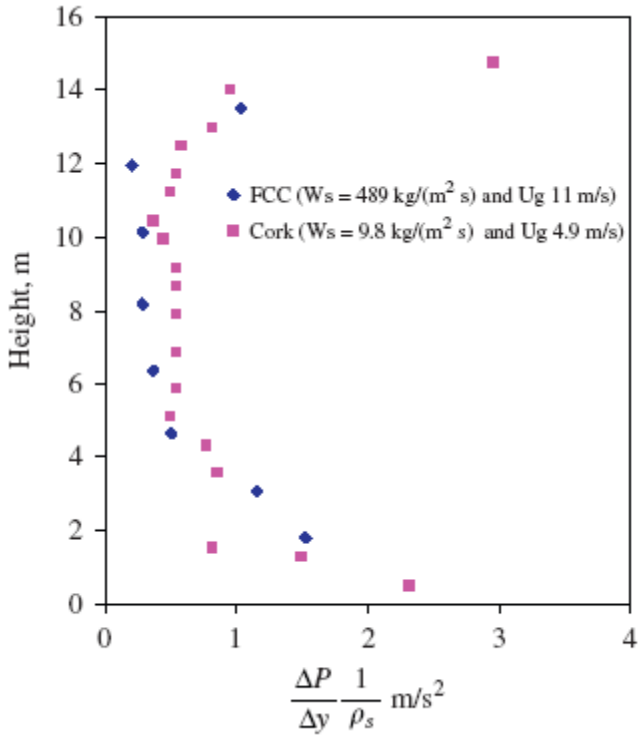

Figure 6. Comparison of axial profile of pressure drop/particle density and solid volume fraction for PSRI data (Knowlton et al., 1995) and NETL data (Mei et al., 2003), based on the approximate mixture momentum balance (Jiradilok et al., 2008)

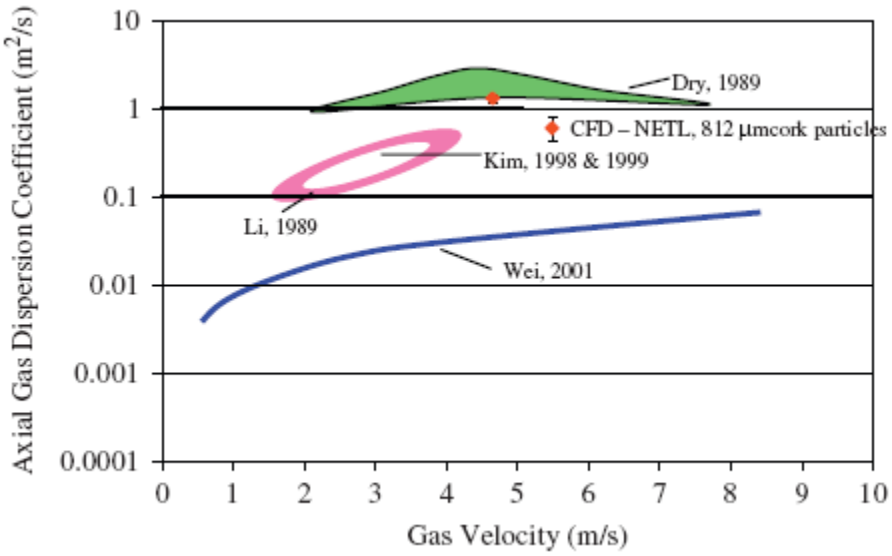

Figure 7. Effect of gas velocity on experimental and computed axial gas dispersion coefficients
(Jiradilok et al, 2007; Dry & White, 1989; Kim & Namkung, 1998, 1999; Li & Weinstein, 1989; Wei et al., 2001)
(Jiradilok et al., 2008)

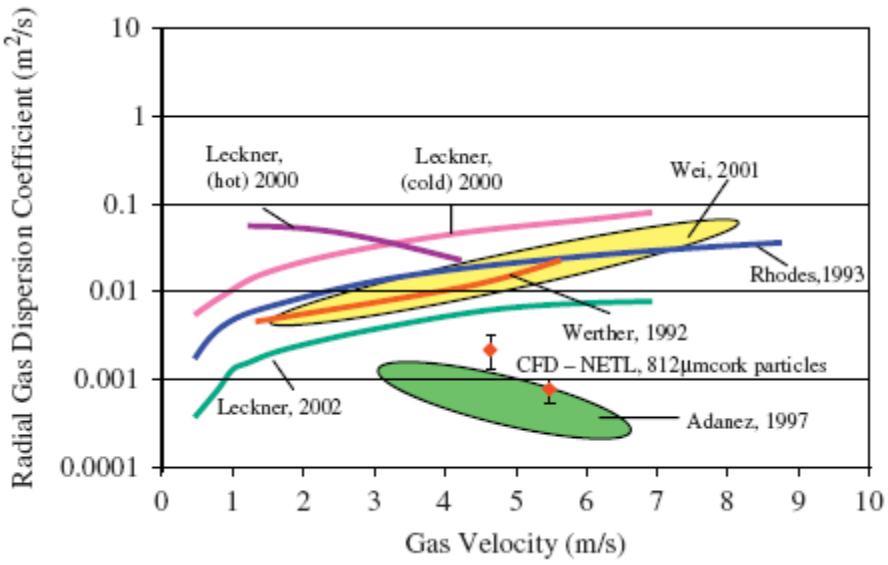

Figure 8. Effect of gas velocity on experimental and computed radial gas dispersion coefficients
(Jiradilok et al., 2007; Leckner et al., 2000, 2002; Werther et al., 1992; Wei et al., 2001; Rhodes et al., 1993; Adanez et al., 1997)
(Jiradilok et al., 2008)

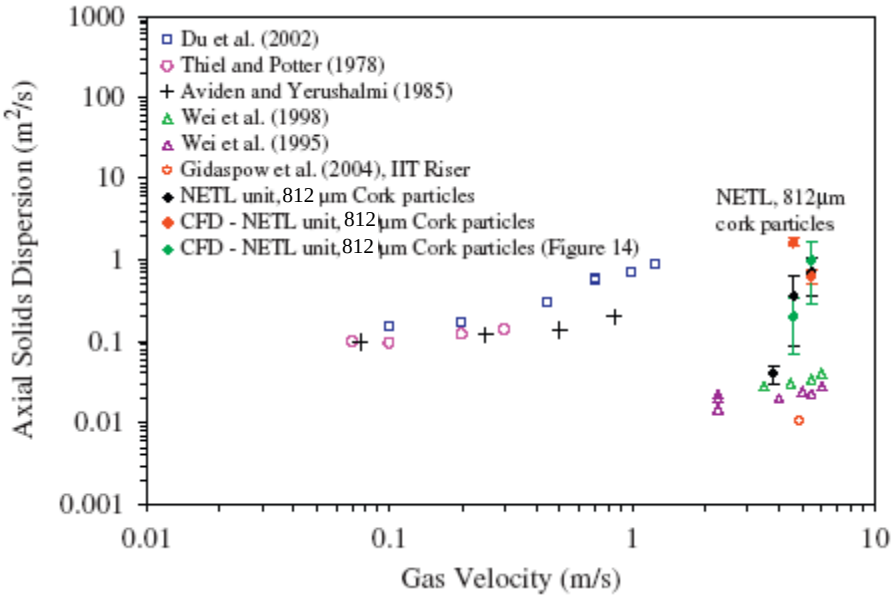

Figure 9. Effect of gas velocity on experimental and computed axial solids dispersion coefficients
(Jiradilok et al., 2007; Thiel and Potter, 1978; Wei et al., 1995, 1998 b; Avidan & Yerushalmi, 1985; Du et al., 2002; Gidaspow et al., 2004)
(Jiradilok et al., 2008)

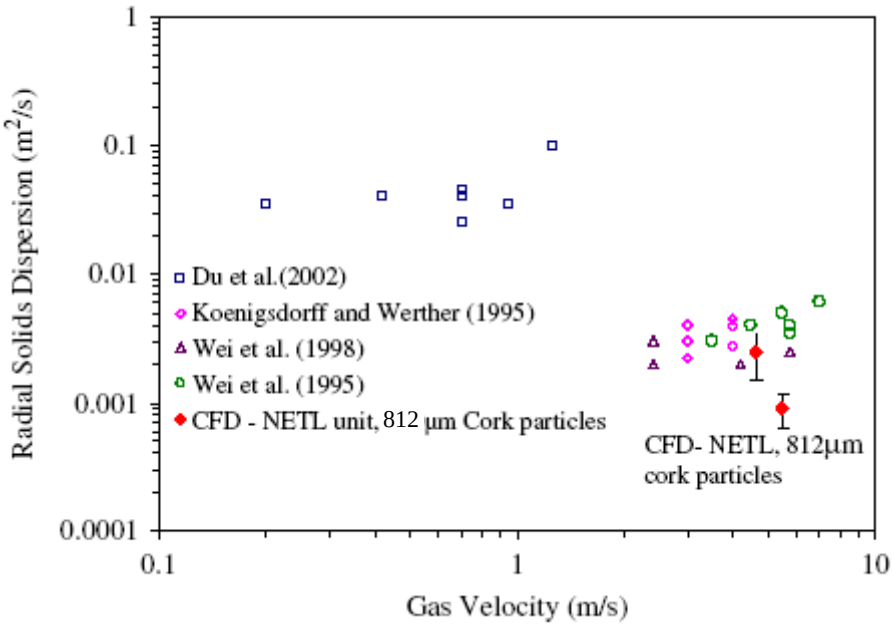

Figure 10. Effect of gas velocity on experimental and computed radial solids dispersion coefficients

(Jiradilok et al., 2007; Du et al., 2002; Koenigsdorff & Werther, 1995; Wei et al., 1995, 1998 b)
(Jiradilok et al., 2008)

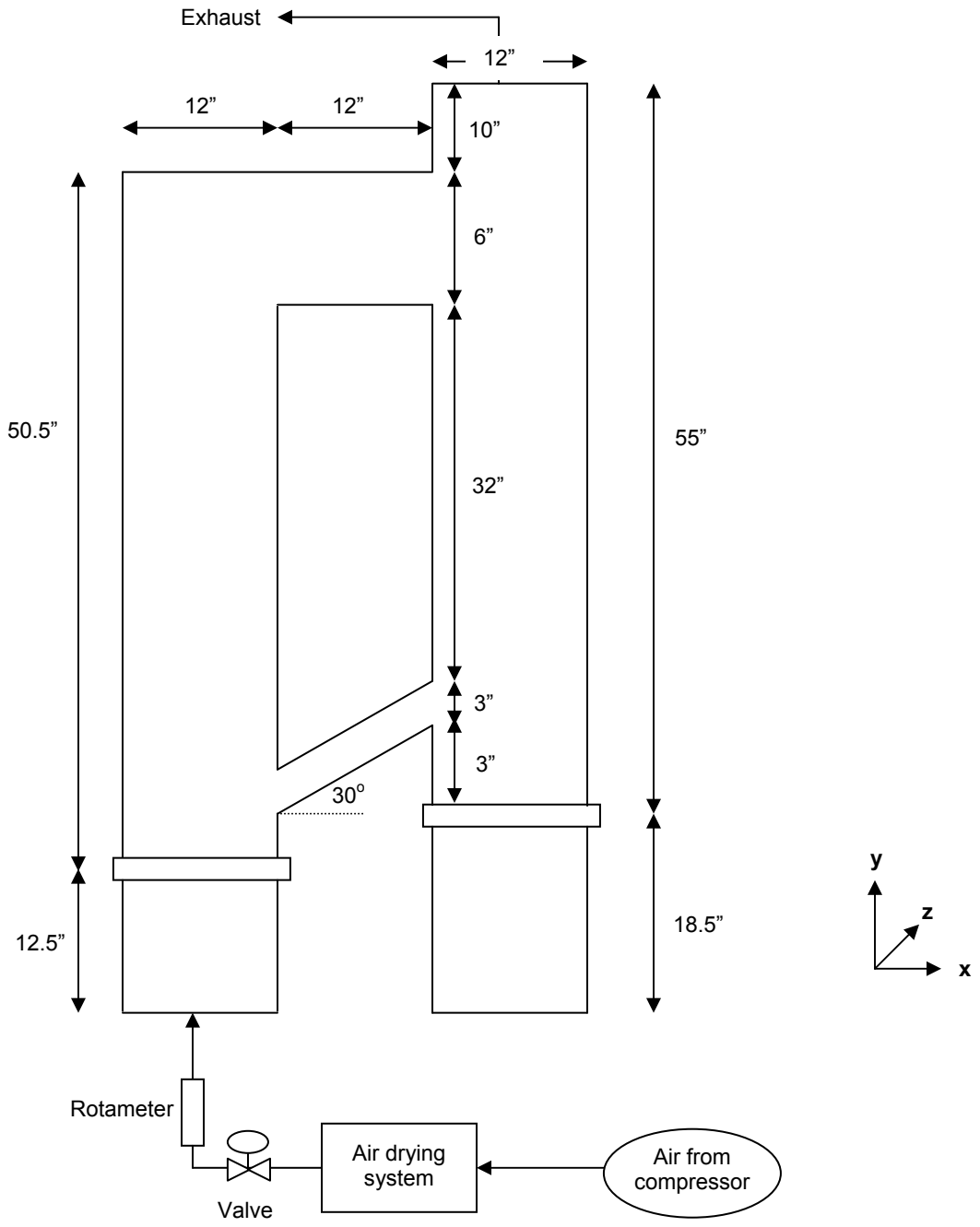

Figure 11. Schematic diagram of the IIT two-dimensional circulating fluidized bed (Kashyap, 2009)

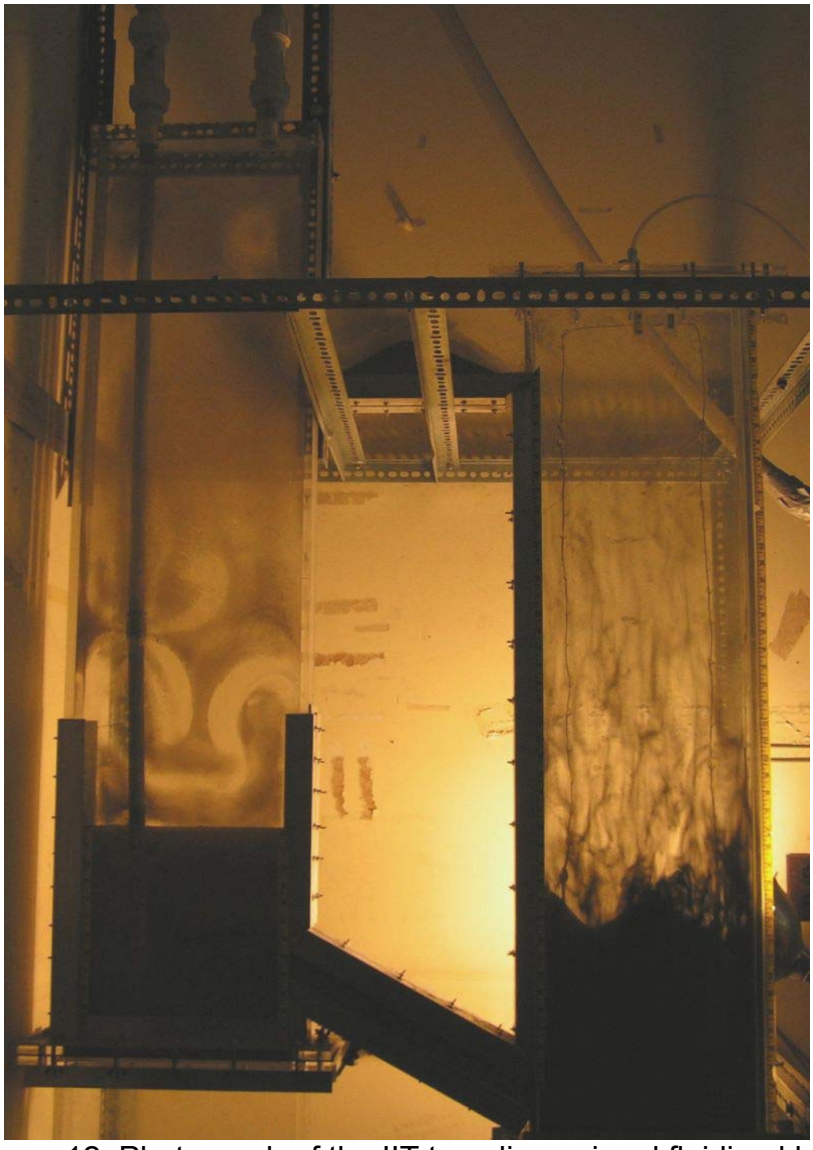

Figure 12. Photograph of the IIT two-dimensional fluidized bed (Kashyap, 2009)

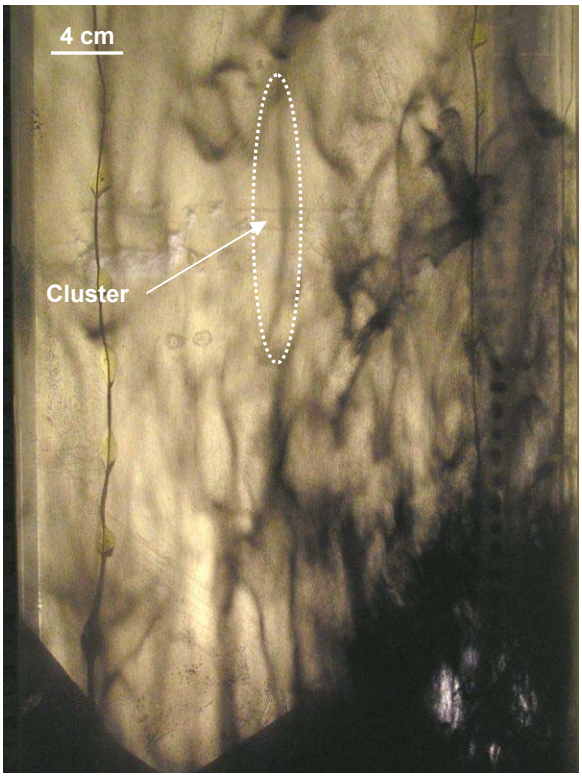

(A)

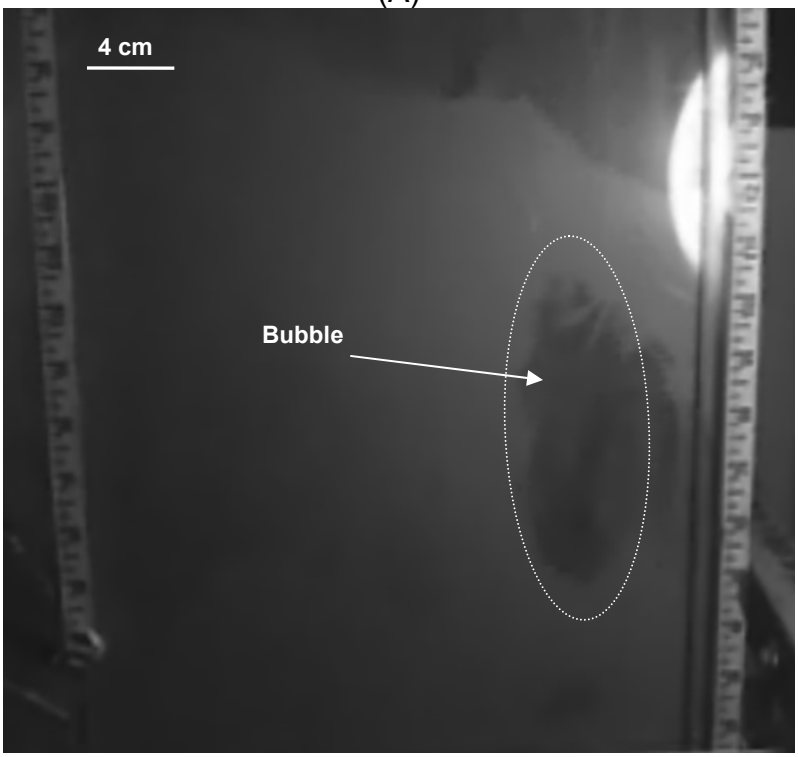

(B)

Figure 13. Typical (A) cluster and (B) bubble formation by 75 μm FCC particles in the IIT two-dimensional fluidized bed
(Kashyap, 2009)

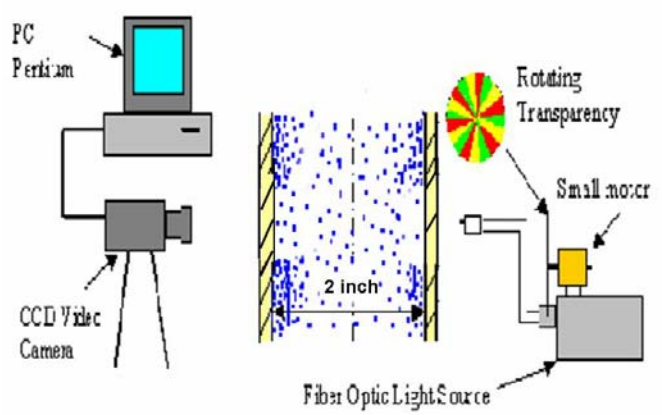

Figure 14. Particle image velocimetry (PIV) measurement system (Kashyap, 2009)

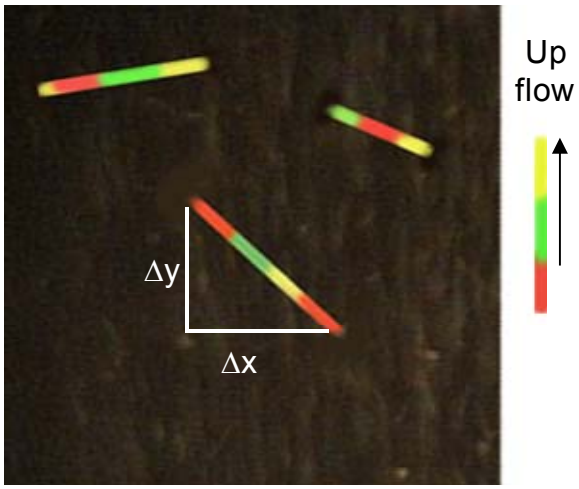

Figure 15. Sketch of the typical streak images captured by the CCD camera (Kashyap, 2009)

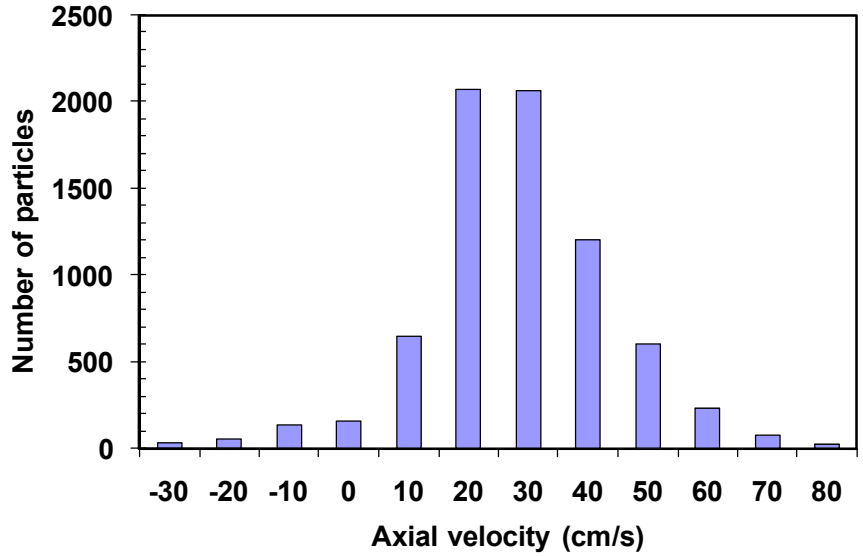

(a)

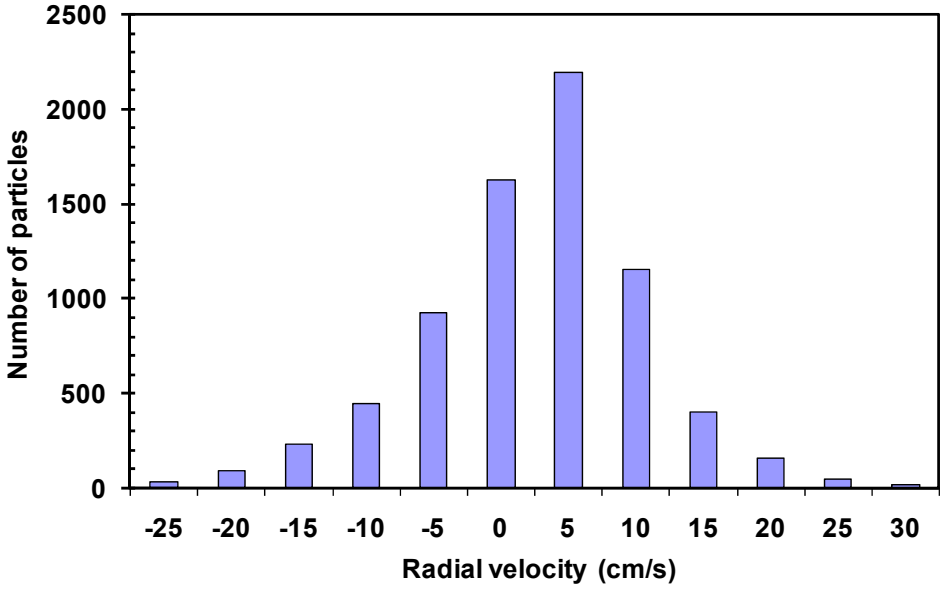

(b)

Figure 16. Instantaneous velocities in the (a) axial and (b) radial directions at H = 69.85 cm, U_g = 46.67 cm/s and t = 1/250 s
(Kashyap, 2009)

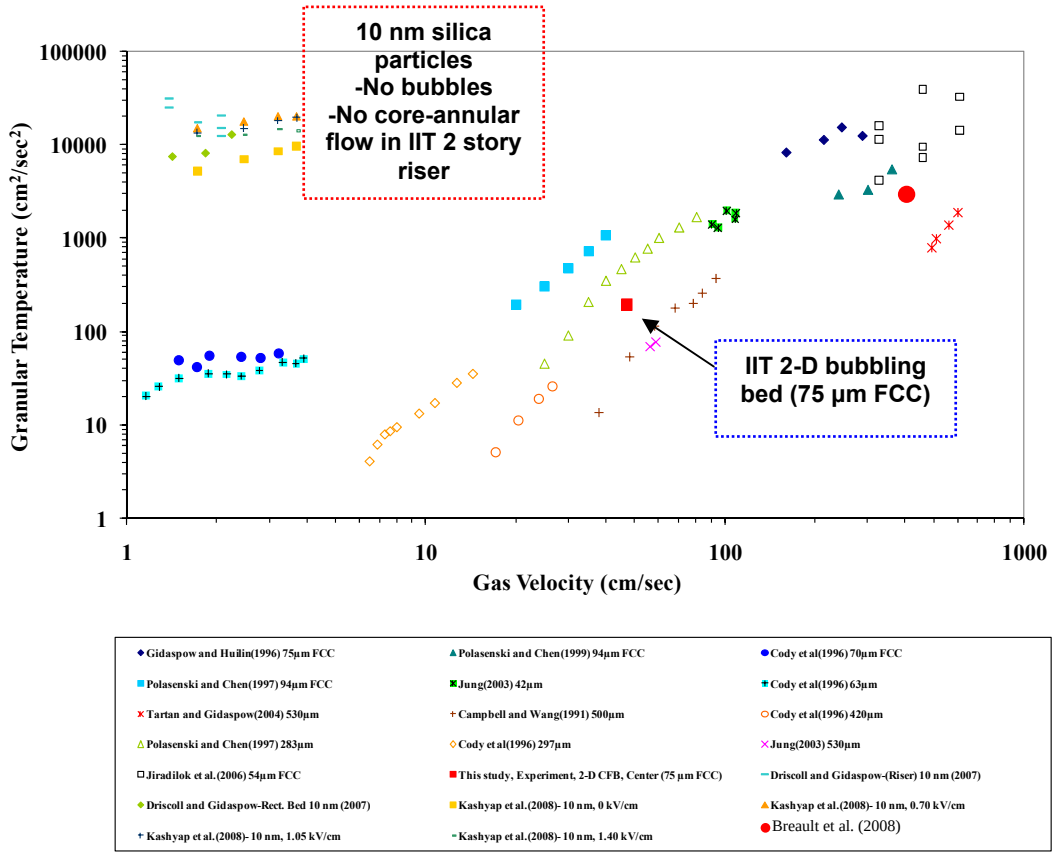

Figure 17. Comparison of granular temperatures obtained by various authors in different fluidized bed systems
(Breault et al., 2008; Campbell & Wang, 1991; Cody et al., 1996; Driscoll & Gidaspow, 2007; Gidaspow & Huilin, 1996; Jiradilok et al., 2006 a; Jung, 2003; Kashyap et al., 2008; Polashenski & Chen, 1997; Polashenski & Chen, 1999; Tartan & Gidaspow, 2004)

(Kashyap, 2009)

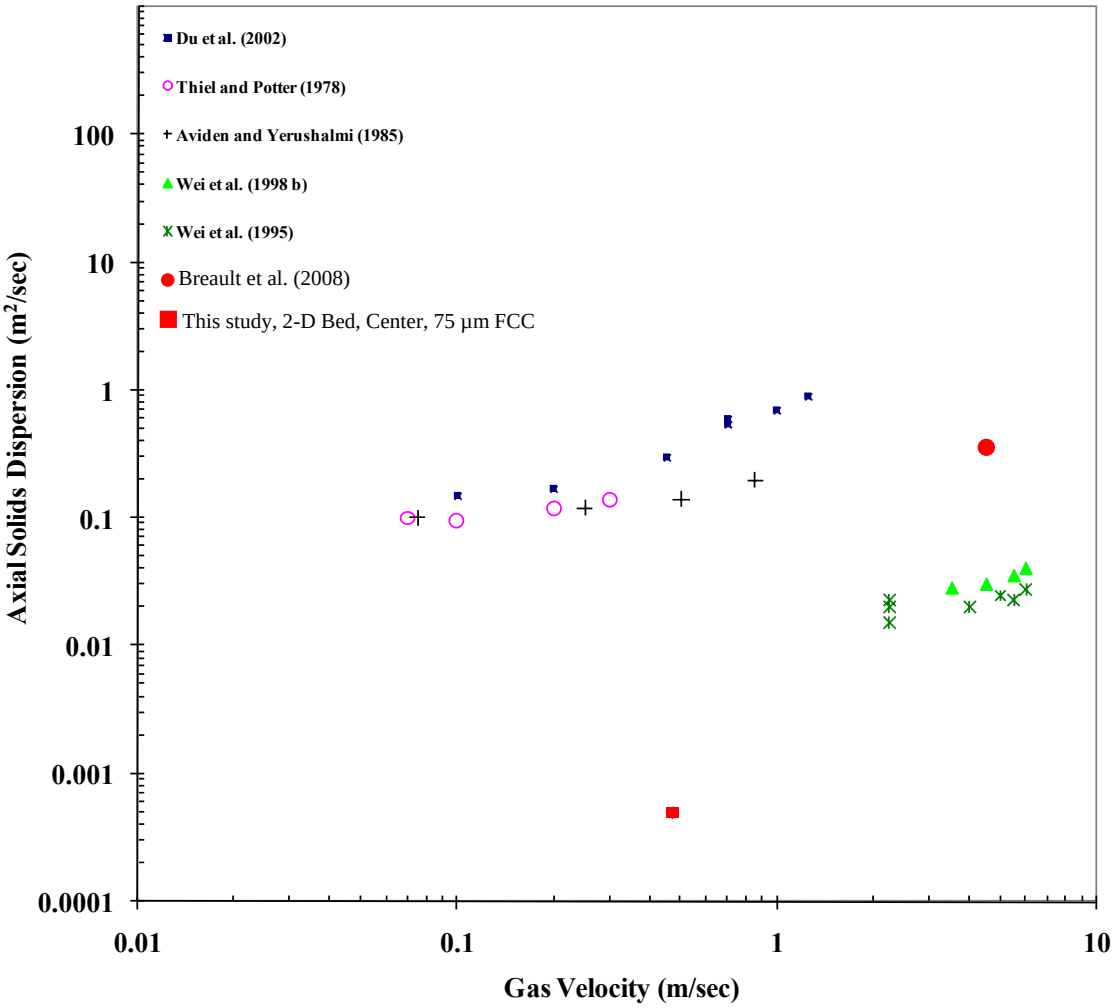

Figure 18. Comparison of axial solid dispersion coefficients obtained by various authors in different fluidized bed systems (Aviden and Yerushalmi, 1985; Breault et al., 2008; Du et al., 2002; Thiel and Potter, 1978; Wei et al., 1995, 1998 b)

(Kashyap, 2009)

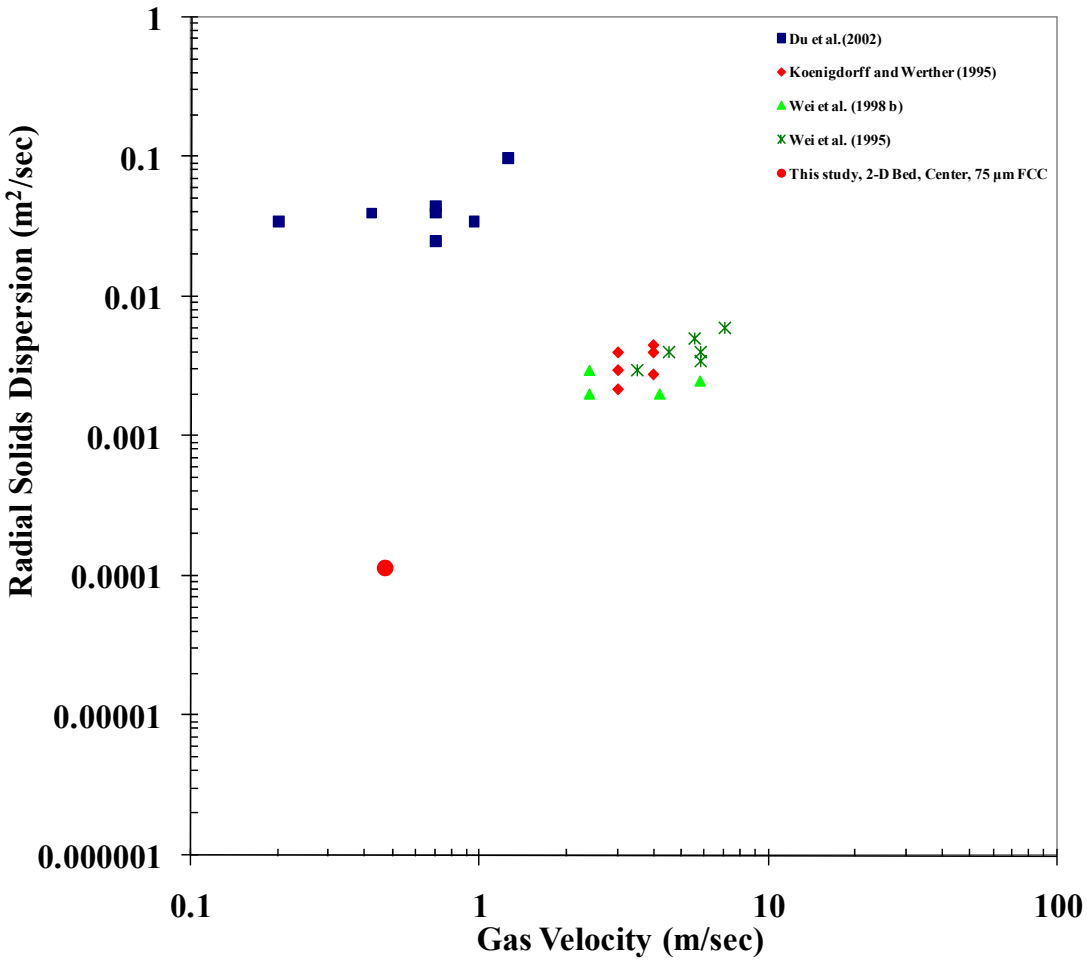

Figure 19. Comparison of radial solid dispersion coefficients obtained by various authors in different fluidized bed systems
(Du et al., 2002; Koenigdorff and Werther, 1995; Wei et al., 1995, 1998 b)

(Kashyap, 2009)

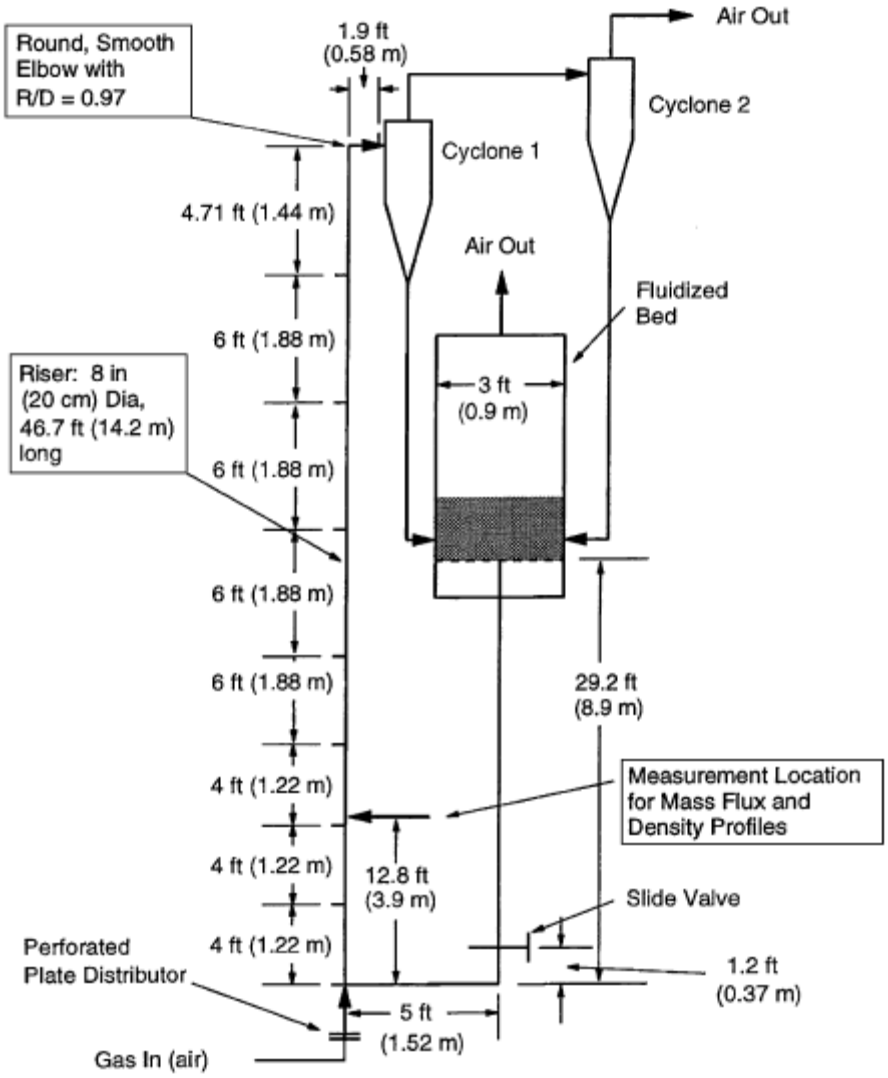

Figure 20. Schematic diagram of a 20 cm diameter circulating fluidized bed test unit for the Fluidization VII benchmark test (Chalermsinsuwan et al., 2009 b)

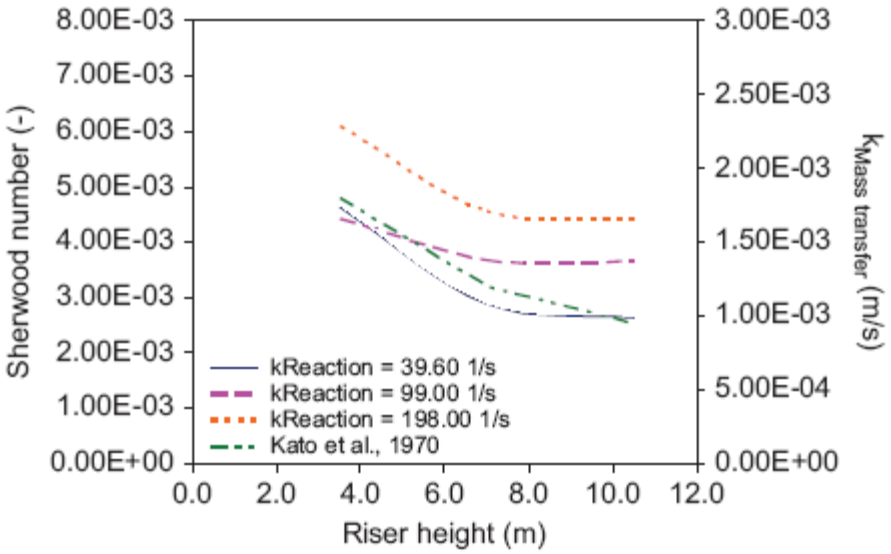

Figure 21. Effect of riser height on computed Sherwood numers and mass transfer coefficients
(Chalermsinsuwan et al., 2009 b)

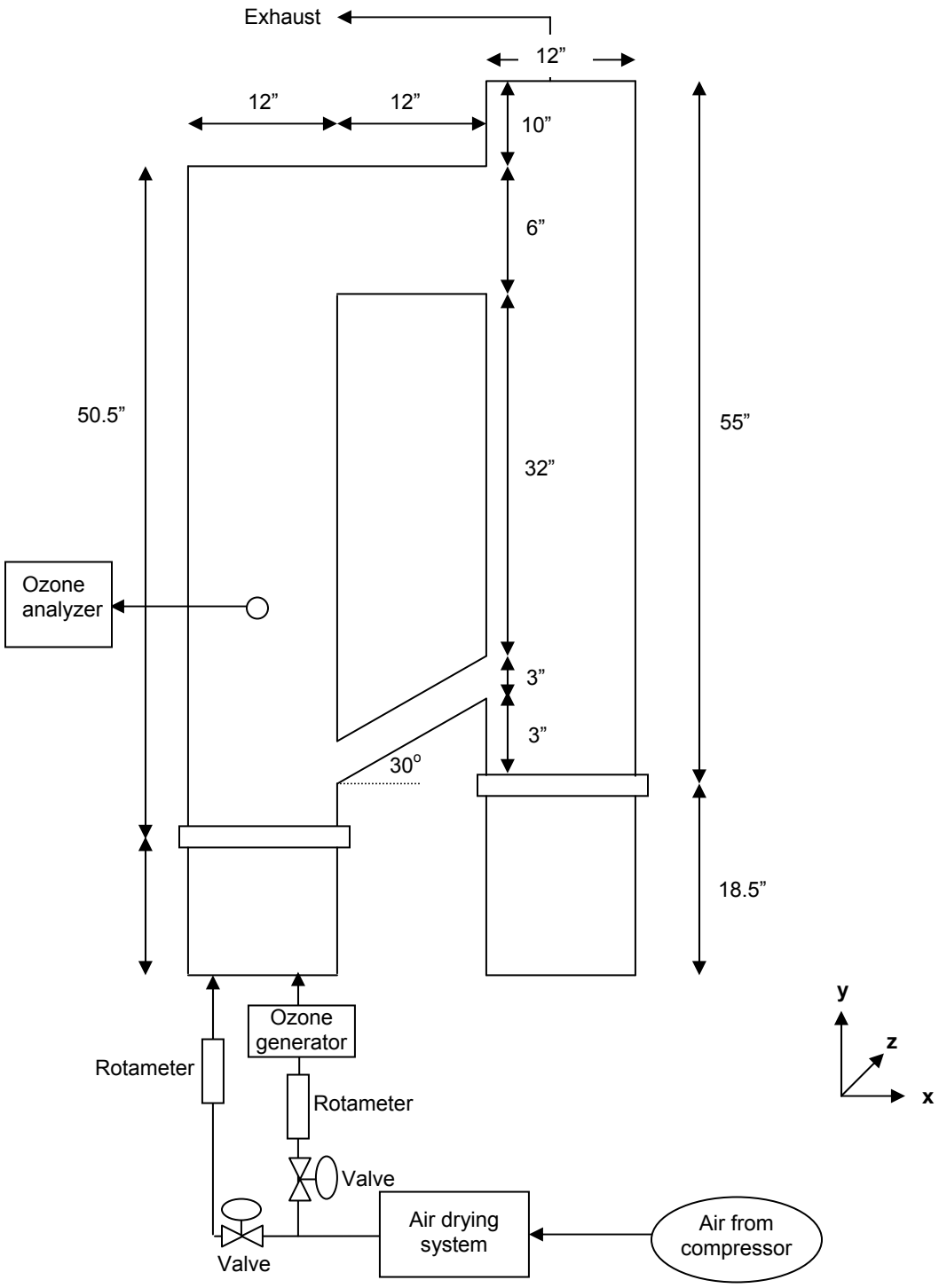

Figure 22. Schematic diagram of the IIT two-dimensional circulating fluidized bed, modified for the measurement of mass transfer coefficients, using the ozone decomposition reaction
(Kashyap, 2009)

Figure 23. Photograph of the IIT two-dimensional fluidized bed system for the measurement of ozone concentrations with ozone decomposition reaction (Kashyap, 2009)

Figure 24. Ozone generator used for the measurement of mass transfer coefficients in the IIT two-dimensional fluidized bed
(Kashyap, 2009)

Figure 25. Ozone analyzer used for the measurement of mass transfer coefficient in the IIT two-dimensional fluidized bed
(Kashyap, 2009)

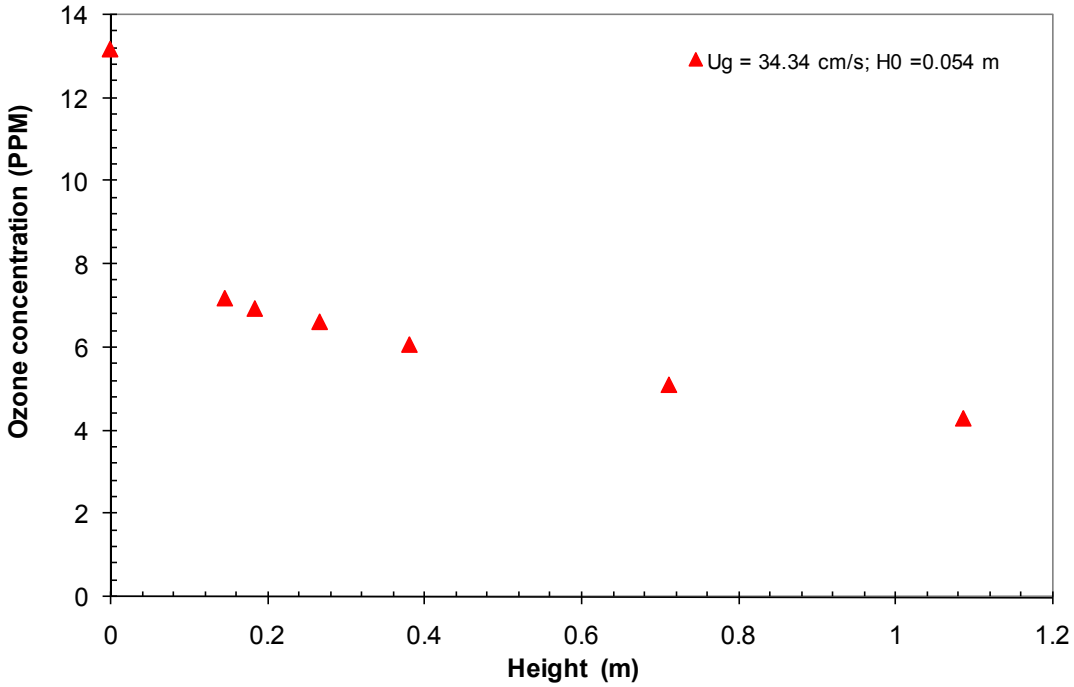

Figure 26. Measured ozone concentrations along the length of the reactor, at a superficial gas velocity of 34.34 cm/s
(Kashyap, 2009)

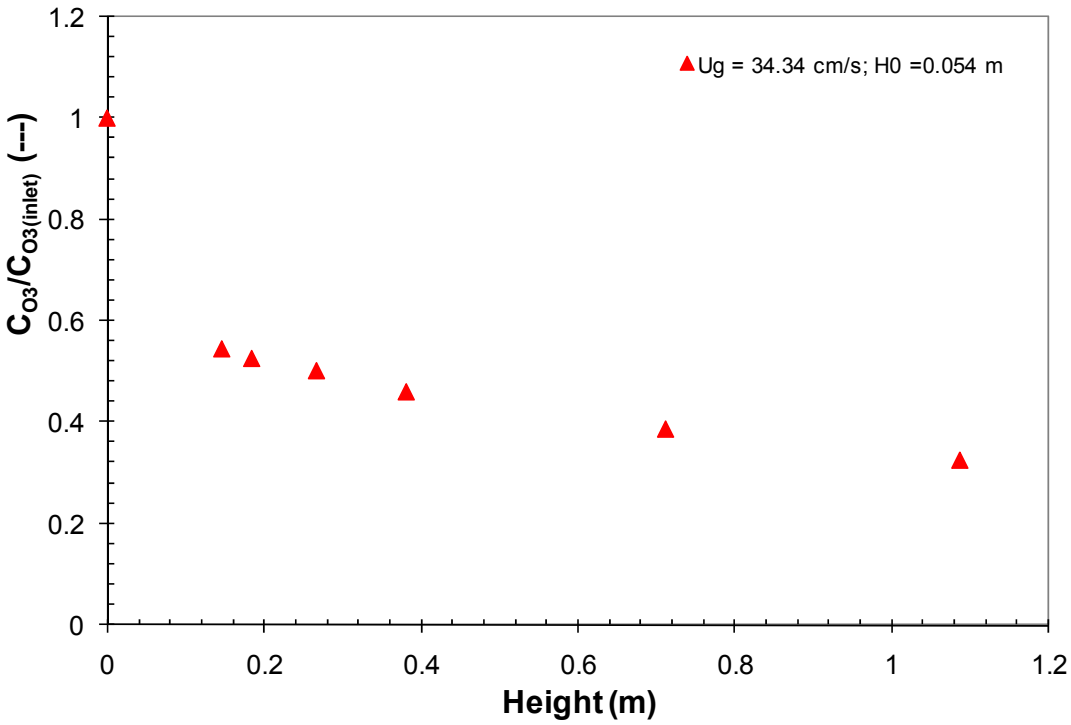

Figure 27. Ratios of local to the inlet ozone concentrations along the length of the reactor, at a superficial gas velocity of 34.34 cm/s (Kashyap, 2009)

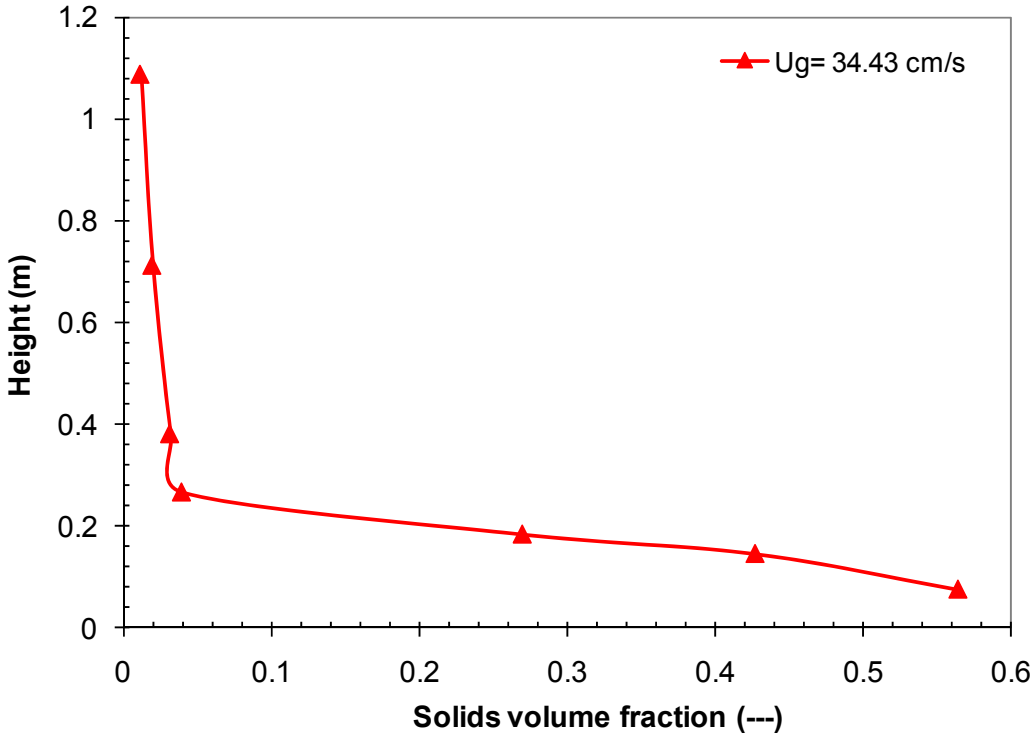

Figure 28. Axial variation of solids volume fraction at a superficial gas velocity of 34.34 cm/s
(Kashyap, 2009)

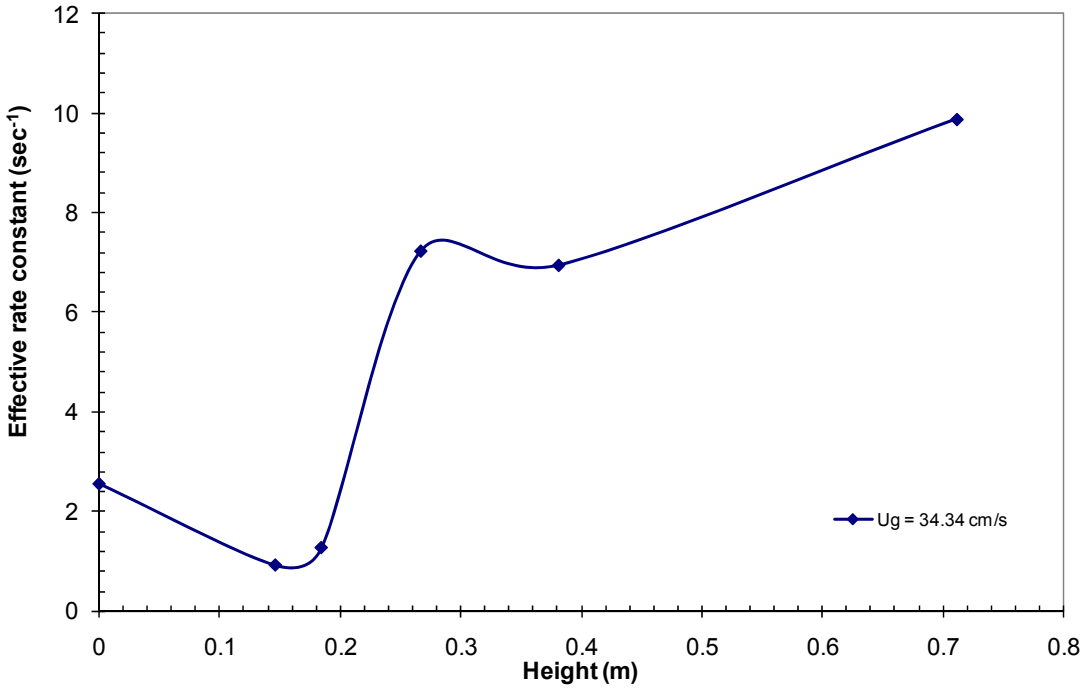

Figure 29. Axial variation of the effective rate constant at a superficial gas velocity of 34.34 cm/s
(Kashyap, 2009)

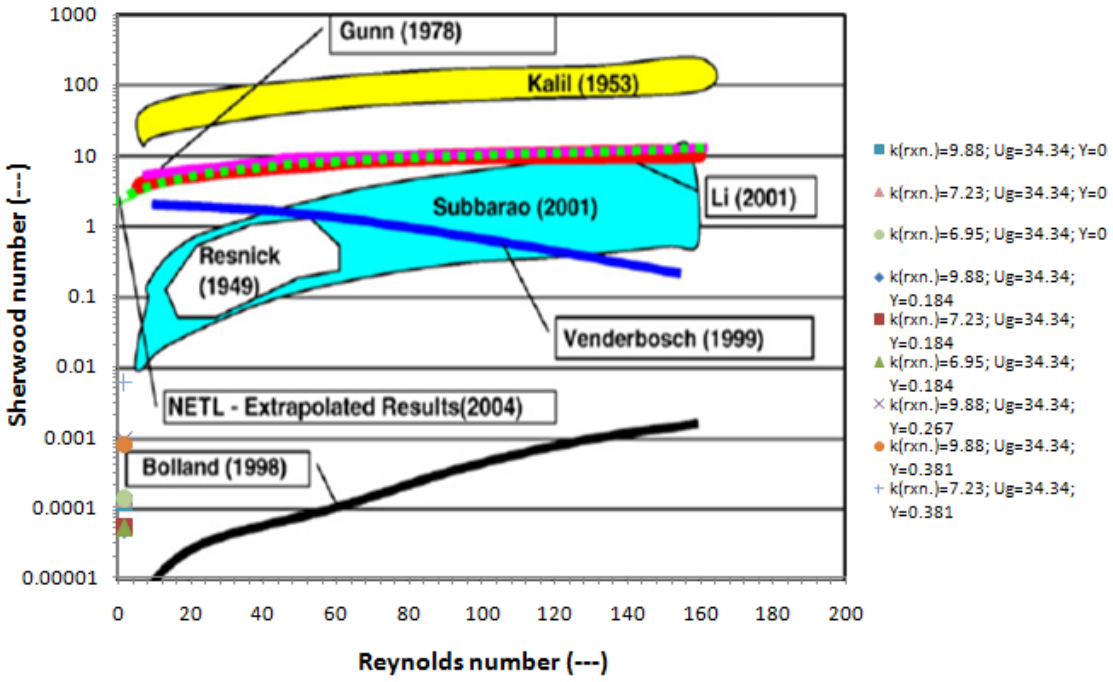

Figure 30. Comparison of the measured Sherwood numbers with the literature values. Reaction rate constant ($k_{reaction}$) is in sec^{-1}; superficial gas velocity (U_g) is in cm/s; height in the fluidized bed (Y) is in meter (Kashyap, 2009)

Table 1. Kinetic theory based hydrodynamic model

Conservation of mass or continuity equations

1. Gas phase:

$$\frac{\partial(\rho_g \varepsilon_g)}{\partial t} + \nabla \cdot (\rho_g \varepsilon_g v_g) = 0$$

2. Solid phase:

$$\frac{\partial(\rho_s \varepsilon_s)}{\partial t} + \nabla \cdot (\rho_s \varepsilon_s v_s) = 0$$

Conservation of momentum equations

1. Gas phase

$$\frac{\partial(\rho_g \varepsilon_g v_g)}{\partial t} + \nabla \cdot (\rho_g \varepsilon_g v_g v_g) = -\varepsilon_g \nabla P + \nabla \cdot \bar{\bar{\tau}}_g - \beta_B (v_g - v_s) + \varepsilon_g \rho_g g + \dot{m}_g \tilde{v}_g$$

2. Solid phase

$$\frac{\partial(\rho_s \varepsilon_s v_s)}{\partial t} + \nabla \cdot (\rho_s \varepsilon_s v_s v_s) = -\varepsilon_s \nabla P - \nabla P_s + \nabla \cdot \bar{\bar{\tau}}_s + \beta_B (v_g - v_s) + \varepsilon_s (\rho_s - \rho_g) g + \dot{m}_s \tilde{v}_s$$

(3)

Conservation of energy equations

1. Gas phase

$$\frac{\partial}{\partial t}(\varepsilon_g \rho_g h_g) + \nabla.(\varepsilon_g \rho_g v_g h_g) = -\varepsilon_g \frac{\partial p_g}{\partial t} + \tau_g : \nabla.v_g + S_g + Q_{sg}$$

with, $h_g = \int c_{pg} dT_g$

2. Solid phase

$$\frac{\partial}{\partial t}(\varepsilon_s \rho_s h_s) + \nabla.(\varepsilon_s \rho_s v_s h_s) = -\varepsilon_s \frac{\partial p_s}{\partial t} + \tau_s : \nabla.v_s + S_s + Q_{gs}$$

with, $h_s = \int c_{ps} dT_s$

Conservation of species equations (i=O_3, O_2 and N_2 (air))

$$\frac{\partial}{\partial t}(\varepsilon_g \rho_g y_i) + \nabla.(\varepsilon_g \rho_g v_g y_i) = r_i$$

Constitutive equations

1) Definitions

$$\varepsilon_g + \varepsilon_s = 1$$

2) Gas Pressure

$$P_g = \rho_g \tilde{R} T_g$$

3) Stress Tensors

Gas phase:

$$\tau_g = \varepsilon_g \mu_g [\nabla v_g + (\nabla v_g)^T] - \frac{2}{3} \varepsilon_g \mu_g (\nabla.v_g) I$$

Solid phase:

$$\tau_s = \varepsilon_s \mu_s [\nabla v_s + (\nabla v_s)^T] - \varepsilon_s (\xi_s - \frac{2}{3}\mu_s)(\nabla . v_s) I$$

4) Collisional dissipation os solid fluctuation energy

$$\gamma_s = 3(1-e^2)\varepsilon_s^2 \rho_s g_o \theta \left(\frac{4}{d_s}\sqrt{\frac{\theta}{\pi}} - \nabla \cdot v_s \right)$$

5) Solid phase pressure

$$P_s = \rho_s \varepsilon_s \theta [1 + 2(1+e) g_o \varepsilon_s]$$

6) Solid phase shear viscosity

$$\mu_s = \frac{2\mu_{s_{dil}}}{(1+e)g_0}\left[1 + \frac{4}{5}(1+e) g_o \varepsilon_s\right] + \frac{4}{5}\varepsilon_s^2 \rho_s d_s g_o (1+e)\sqrt{\frac{\theta}{\pi}}$$

7) Solid phase bulk viscosity

$$\lambda_s = \frac{4}{3}\varepsilon_s^2 \rho_s d_s g_o (1+e)\sqrt{\frac{\theta}{\pi}}$$

where, g_0 is the radial distribution function and μ_{sdil} is the particle phase dilute viscosity.

$$g_o = \left[1 - \left(\frac{\varepsilon_s}{\varepsilon_{s,\max}}\right)^{1/3}\right]^{-1}$$

$$\mu_{s_{dil}} = \frac{5\sqrt{\pi}}{96}\rho_p d_p \theta^{1/2}$$

Conservation of fluctuating energy equation for particles ($\theta = 1/3 \cdot \langle C^2 \rangle$)

$$\frac{3}{2}\left[\frac{\partial}{\partial t}(\varepsilon_s \rho_s \theta) + \nabla \cdot (\varepsilon_s \rho_s v_s \theta)\right] = \left(-\nabla P_s \bar{\bar{I}} + \bar{\bar{\tau}}_s\right) : \nabla v_s + \nabla \cdot (\kappa_s \nabla \theta) - \gamma_s$$

Granular conductivity of fluctuating energy ($q = -k\nabla\theta$)

$$\kappa = \frac{2}{(1+e)g_0}\left[1 + \frac{6}{5}(1+e) g_o \varepsilon_s\right]^2 \kappa_{dil} + 2\varepsilon_s^2 \rho_s d_s g_o (1+e)\sqrt{\frac{\theta}{\pi}}$$

where, $\kappa_{dil} = \frac{75}{384}\sqrt{\pi \rho_s} d_s \theta^{1/2}$

Gas–solid drag coefficient

Normal drag:

for $\varepsilon_g < 0.8$ (based on the Ergun equation)

$$\beta = 150\frac{\varepsilon_s^2 \mu_g}{\varepsilon_g^2 d_p^2} + 1.75\frac{\rho_g \varepsilon_s}{\varepsilon_g d_p}\left|\upsilon_g - \upsilon_s\right|$$

for $\varepsilon_g \geq 0.8$ (based on the empirical correlation)

$$\beta = \frac{3}{4} C_d \frac{\rho_g \varepsilon_s \left| \upsilon_g - \upsilon_s \right|}{d_p} \varepsilon_g^{-2.65}$$

EMMS drag

for $\varepsilon_g < 0.74$

$$\beta = 150 \frac{\varepsilon_s^2 \mu_g}{\varepsilon_g^2 d_p^2} + 1.75 \frac{\rho_g \varepsilon_s}{\varepsilon_g d_p} \left| \upsilon_g - \upsilon_s \right|$$

for $\varepsilon_g \geq 0.74$

$$\beta = \frac{3}{4} C_d \frac{\rho_g \varepsilon_s \varepsilon_g \left| \upsilon_g - \upsilon_s \right|}{d_p} \omega(\varepsilon_g)$$

when, $0.74 \leq \varepsilon_g \leq 0.82$, $\omega(\varepsilon_g) = -0.5760 + \dfrac{0.0214}{4(\varepsilon_g - 0.7463)^2 + 0.0044}$

when, $0.82 \leq \varepsilon_g \leq 0.97$, $\omega(\varepsilon_g) = -0.0101 + \dfrac{0.0038}{4(\varepsilon_g - 0.7789)^2 + 0.0040}$

when, $\varepsilon_g > 0.97$, $\omega(\varepsilon_g) = -31.8295 + 32.8295 \varepsilon_g$

with,

$$C_d = \frac{24}{\mathrm{Re}_p} \left[1 + 0.15 \mathrm{Re}_p^{0.697} \right] \quad \text{for} \quad \mathrm{Re}_p < 1000$$

$$C_d = 0.44 \quad \text{for} \quad \mathrm{Re}_p > 1000$$

$$\mathrm{Re}_p = \frac{\varepsilon_g \rho_g d_p \left| v_g - v_s \right|}{\mu_g}$$

Boundary conditions for particle phase (Johnson and Jackson, 1987)

1) Velocity

$$\mathrm{v}_{s,w} = -\frac{6 \mu_s \varepsilon_{s,\max}}{\sqrt{3} \pi \phi \rho_s \varepsilon_s g_0 \sqrt{\theta}} \frac{\partial \mathrm{v}_{s,w}}{\partial \mathrm{n}}$$

2) Granular Temperature

$$\theta_w = -\frac{\kappa \theta}{\gamma_w} \frac{\partial \theta_w}{\partial n} + \frac{\sqrt{3} \pi \phi \rho_s \varepsilon_s \vec{u}_{s,slip}^2 g_0 \theta^{3/2}}{6 \varepsilon_{s,\max} \gamma_w} \qquad \text{where} \qquad \gamma_w = \frac{\sqrt{3} \pi \left(1 - e_w^2\right) \varepsilon_s \rho_s g_0 \theta^{3/2}}{4 \varepsilon_{s,\max}}$$

Boundary conditions for gas phase

$$\mathrm{v}_{x,w} = \mathrm{v}_{y,w} = 0$$

Table 2. System properties and initial conditions for the dispersion and mass transfer coefficient measurements
(Kashyap, 2009)

Dispersion coefficients

Particles used:	FCC
Size of particles, d_p (μm):	75
Density of particles, ρ (kg/m^3)	1674
Initial bed height, H_o (cm)	14
Data acquisition: Position along the "axial or y-direction", Y (cm)	69.85
Data acquisition: Position along the "radial or x-direction"	Center
Data acquisition: Position along the "radially inward or z-direction"	Front wall
Superficial gas velocity, U_g (cm/s)	46.67
Solids flux at 0.7 m ($kg/(m^2$-s))	8.4

Mass transfer coefficients

Particles used:	FCC
Size of particles, d_p (μm):	75
Density of particles, ρ (kg/m^3)	1674
Initial bed height, H_o (cm)	5.4
Data acquisition: Position along the "axial or y-direction", Y (cm)	H_0=0, H_1=14.6, H_2=18.4, H_3=26.7, H_4=38.1, H_5=71.1, H_6=108.6
Data acquisition: Position along the "radial or x-direction"	Center
Data acquisition: Position along the "radially inward or z-direction"	Center
Superficial gas velocity, U_g (cm/s)	34.34

Table 3. Measured laminar and turbulent granular temperatures in the IIT two-dimensional fluidized bed. Mixing is on the level of particles (Kashyap, 2009)

Granular temperature, θ, m^2/s^2			
System	Radial (z) position	Laminar due to individual particle oscillations	Turbulent due to cluster oscillations
2-D CFB, 75 μm FCC particles	Center	1.27×10^{-2}	6.73×10^{-3}

Table 4. Measured axial and radial solids dispersion coefficients in the IIT two-dimensional fluidized bed. Mixing is on the level of particles (Kashyap, 2009)

Dispersion coefficient, m^2/s				
System	Radial (z) position	Type	Axial	Radial
2-D CFB, 75 μm FCC particles	Center	Laminar	3.21×10^{-4}	7.66×10^{-5}
2-D CFB, 75 μm FCC particles	Center	Turbulent	1.77×10^{-4}	3.78×10^{-5}

Table 5. Reaction rate constants equal to the effective rate constants in the free board regime
(Kashyap, 2009)

Calculation of $k_{reaction}$			
Height used for linear equation solving, Y (m)	0.711	0.381	0.267
$k_{reaction}$ (sec^{-1})	9.88	7.23	6.95

Table 6. Calculation of the mass transfer coefficients and Sherwood numbers at different axial positions in the IIT two-dimensional fluidized bed, using additive resistances
(Kashyap, 2009)

(A)

	a_v =	78947.37						
Superficial gas velocity, U_g (cm/s)	$k_{reaction}$ (sec^{-1})	K at the bottom of CFB (sec^{-1})	$k_{mass\ transfer}$ (m/s)	$Sh_{particle}$	$d_{bubble\ (picture)}$ (m)	$Sh_{bubble\ (picture)}$	$Sh_{(diffusion\ limit)}$	$d_{bubble\ (diffusion)}$ (m)
34.34	9.88	2.55	4.35E-05	0.00011	0.11	0.166	2	1.32
34.34	7.23	2.55	4.99E-05	0.00013	0.11	0.191	2	1.15
34.34	6.95	2.55	5.10E-05	0.00013	0.11	0.195	2	1.13

(B)

	a_v =	78947.37						
Superficial gas velocity, U_g (cm/s)	$k_{reaction}$ (sec^{-1})	K in cluster region (Y=0.184m) (sec^{-1})	$k_{mass\ transfer}$ (m/s)	$Sh_{particle}$	$d_{cluster\ (picture)}$ (m)	$Sh_{cluster\ (picture)}$	$Sh_{(diffusion\ limit)}$	$d_{cluster\ (diffusion)}$ (m)
34.34	9.88	1.27	1.84E-05	0.00005	0.14	0.089	2	3.13
34.34	7.23	1.27	1.94E-05	0.00005	0.14	0.095	2	2.96
34.34	6.95	1.27	1.96E-05	0.00005	0.14	0.095	2	2.94

(C)

	a_v =	78947.37						
Superficial gas velocity, U_g (cm/s)	$k_{reaction}$ (sec^{-1})	K in cluster region (Y=0.267m) (sec^{-1})	$k_{mass\ transfer}$ (m/s)	$Sh_{particle}$	$d_{cluster\ (picture)}$ (m)	$Sh_{cluster\ (picture)}$	$Sh_{(diffusion\ limit)}$	$d_{cluster\ (diffusion)}$ (m)
34.34	9.88	7.23	3.42E-04	0.00090	0.14	1.66	2	0.17
34.34	7.23	7.23	----	----	0.14	----	2	----
34.34	6.95	7.23	----	----	0.14	----	2	----